# Quantifying sources, transport, deposition and radiative forcing of black carbon over the Himalayas and Tibetan Plateau

Rudong Zhang[1, 2, 3], Hailong Wang[2], Yun Qian[2], Philip J. Rasch[2], Richard C. Easter[2], Po-Lun Ma[2], Balwinder Singh[2], Jianping Huang[1], and Qiang Fu[1, 3]

[1] Key Laboratory for Semi-Arid Climate Change of the Ministry of Education, College of Atmospheric Sciences, Lanzhou University, Lanzhou 730000, Gansu, China.

[2] Atmospheric Sciences and Global Change Division, Pacific Northwest National Laboratory (PNNL), Richland, WA 99352, USA.

[3] Department of Atmospheric Sciences, Box 351640, University of Washington, Seattle, WA 98195, USA.

Manuscript for submission to *Atmospheric Chemistry and Physics*

Correspondence to: Hailong.Wang@pnnl.gov

## Abstract

Black carbon (BC) particles over the Himalayas and Tibetan Plateau (HTP), both airborne and those deposited on snow, have been shown to affect snowmelt and glacier retreat. Since BC over the HTP may originate from a variety of geographical regions and emission sectors, it is essential to quantify the source-receptor relationships of BC in order to understand the contributions of natural and anthropogenic emissions and provide guidance for potential mitigation actions. In this study, we use the Community Atmosphere Model version 5 (CAM5) with a newly developed source tagging technique, nudged towards the MERRA meteorological reanalysis, to characterize the fate of BC particles emitted from various geographical regions and sectors. Evaluated against observations over the HTP and surrounding regions, the model simulation shows a good agreement in the seasonal variation of the near-surface airborne BC concentrations, providing confidence to use this modeling framework for characterizing BC source-receptor relationships. Our analysis shows that the relative contributions from different geographical regions and source sectors depend on season and location in the HTP. The largest contribution to annual mean BC burden and surface deposition in the entire HTP region is from biofuel and biomass (BB) emissions in South Asia, followed by fossil fuel (FF) emissions from South Asia, then FF from East Asia. The same roles hold for all the seasonal means except for the summer when East Asia FF becomes more important. For finer receptor regions of interest, South Asia BB and FF have the largest impact on BC in Himalayas and Central Tibetan Plateau, while East Asia FF and BB contribute the most to Northeast Plateau in all seasons and Southeast Plateau in the summer. Central Asia and Middle East FF emissions have relatively more important contributions to BC reaching Northwest Plateau, especially in the summer. Although local emissions only contribute about 10% of BC in the HTP, this contribution is extremely sensitive

to local emission changes. Lastly, we show that the annual mean radiative forcing (0.42 W $m^{-2}$) due to BC in snow outweighs the BC dimming effect (-0.3 W $m^{-2}$) at the surface over the HTP. We also find strong seasonal and spatial variation with a peak value of 5 W $m^{-2}$ in the spring over Northwest Plateau. Such a large forcing of BC in snow is sufficient to cause earlier snow melting and potentially contribute to the acceleration of glacier retreat.

## 1 Introduction

Black carbon (BC) is a distinct type of carbonaceous particulate matter mainly emitted from the incomplete combustion of fossil fuels, biofuels and biomass burning. It is the dominant insoluble light-absorbing particulate species, both in the atmosphere and after deposition on snow and ice. In addition to its impact on air quality, BC plays a unique and important role in the climate system through its effect on radiation, clouds and snow albedo, and associated feedbacks that modify atmospheric circulation patterns and/or accelerate the snowmelt and glacier retreat in the Arctic and across the mid-latitudes of the northern hemisphere (Bond et al., 2013).

Modeling studies (e.g., Hansen et al., 2005; Qian et al., 2011) indicate that the climate efficacy of BC in snow is much greater than efficacy of carbon dioxide or other anthropogenic forcers owing to a sequence of positive feedback mechanisms (Warren and Wiscombe, 1980, 1985; Conway et al., 1996; Hansen and Nazarenko, 2004; Jacobson, 2004; Flanner et al., 2007; Ye et al., 2012; Hadley and Kirchstetter, 2012; Doherty et al., 2014). Flanner et al. (2009) demonstrated that the global annual BC snow-albedo effect (darkening) outweighs the aerosol (BC and organic matter) dimming effect (i.e., reduced the downwelling irradiance reaching the surface) by a factor of about 6. The snow/ice-covered Himalayas and Tibetan Plateau (HTP) region is more prone to these BC effects than other regions because of the surrounding two major

47 BC source regions, East Asia and South Asia, at present and likely in the future (e.g., Bond et al.,
48 2007; Ohara et al., 2007; Xu et al., 2009; Lamarque et al., 2010; Menon et al., 2010).

49 The HTP, often referred to as the Third Pole, has received much less scientific attention
50 than the Polar Regions (Qiu, 2008), although it is the highest and largest plateau that stores one
51 of the largest ice masses of the Earth system. The HTP also has a large area of seasonal and
52 permanent snow cover and represents the most sensitive and visible indicator of climate change
53 with its unique location for complex interactions among the atmosphere, hydrosphere and
54 cryosphere (e.g., Pu et al., 2007; Xu et al., 2009; Yao et al., 2012). The glaciers and the
55 associated snowmelt over the HTP have a great potential to modify the regional hydrology and to
56 trigger natural hazards that impact a large portion of the population in and around the region (e.g.,
57 Barnett et al., 2005; Singh and Bengtsson, 2004; Xu et al., 2008; Kaser et al., 2010; Immerzeel et
58 al., 2010; Yao et al., 2012; Bolch et al., 2012). The HTP also exerts profound influences on
59 atmospheric circulation patterns and climate through mechanical and thermal effects due to its
60 large area, highly elevated topography and geographical location in the Earth system (Yeh et al.,
61 1957; Manabe and Terpstra, 1974; Ye and Gao, 1979; Yanai et al., 1992; Ye and Wu, 1998; Wu
62 et al., 2012). The HTP acts as a giant wall across the Eurasian continent that blocks cold
63 outbreaks from high latitudes in winter and confines the winter monsoon to eastern and southern
64 Asia, while in summer the HTP serves as a huge heat source through the strong surface sensible
65 heating and latent heating over central and eastern Plateau (Wu et al., 2012).

66 Under the background of global warming, the climate of the HTP is changing rapidly. For
67 example, the surface sensible heat flux has weakened in recent decades, mainly due to global
68 warming (Duan and Wu, 2008). Observational evidence indicated that the surface air
69 temperatures on the HTP have increased about 1.8°C over the past 50 years (Wang et al., 2008),

while the large area at elevations above 4000 m has warmed at 0.3°C per decade in the past three decades (Xu et al., 2009). A number of recent studies reported that glaciers on the HTP have undergone widespread losses at an increasing rate in past decades (e.g., Qin et al., 2006; Li et al., 2008; Kang et al., 2010; Bolch et al., 2012) and have undergone accelerated retreat in recent years (Yao et al., 2007). The rapid warming and the accelerated glacier retreat have been primarily attributed to increasing greenhouse gases (e.g., Duan et al., 2006; Ren et al., 2006), but other factors may be partly responsible for the accelerated warming over the HTP, such as atmospheric heating by absorbing aerosols, land use changes, and reduction of snow albedo induced by light-absorbing impurities in snow (Kang et al., 2000; Prasad and Singh 2007; Ramanathan et al., 2007; Flanner et al., 2007, 2009; Yasunari et al., 2010; Xu et al., 2009; Qian et al., 2011, 2015). Lau et al. (2006, 2010) proposed and demonstrated the Elevated Heat Pump mechanism, whereby heating induced by airborne BC and dust absorption can strengthen local circulations and lead to a northward shift of the monsoon rain belt, widespread enhanced warming over the HTP, and accelerated snowmelt and glacier retreat. Previous observational and modeling studies have indicated that BC deposition on snow and ice, which has a rapidly increasing trend in recent years, has been a significant contributor to the early snowmelt and rapid glacier retreat over the HTP (e.g., Flanner et al., 2007, 2009; Ming et al., 2008; Xu et al., 2009; Kaspari et al., 2011; Menon, et al., 2010; Qian et al., 2011, 2015; Wang et al., 2015). Flanner et al. (2007) found that the largest regional annual mean forcing due to BC in snow is located in the HTP. Xu et al. (2009) and Lau et al. (2010) suggested that the BC in snow/ice may be partly responsible for the observed acceleration of glacier retreat in the HTP.

Understanding the role of BC in accelerating snow-cover reduction and glacier retreat is becoming increasingly important. Over 60% of BC in the present-day atmosphere originates

93 from anthropogenic activities (e.g., Bond et al., 2007; Lamarque et al., 2010). Reduction of
94 emissions from BC-rich sources represents a potential mitigation strategy to slow down the
95 climate change because BC has a positive radiative forcing but a short atmospheric lifetime
96 (Bond et al., 2013). Since BC over the HTP may originate from a variety of geographical regions
97 and emission sectors, it is essential to quantify the source-receptor relationships of BC in order to
98 understand the contributions of open fire and anthropogenic emission sectors to BC over the
99 HTP. This exercise is also essential to provide guidance for potential mitigation actions.

100 Some studies have used the conventional back-trajectory approach to identify possible
101 source regions for both airborne BC and that deposited on snow and ice, by tracking air mass
102 reaching sampling sites over the HTP (e.g., Ming et al., 2008, 2009; Cao et al., 2009; Bonasoni
103 et al., 2010; Zhao et al., 2013; Zhang et al., 2013). Lu et al. (2012) developed a novel back-
104 trajectory approach to analyze the origin of BC transported to the HTP during 1996-2010. They
105 derived the overall transport characteristics of BC to the HTP and showed the spatial distribution
106 of sources for BC reaching the HTP region based on a large set of seven-day back trajectories
107 arriving at the given height (i.e., 500 m) and receptor locations, BC emissions and transport
108 efficiencies. The statistical analysis of trajectories has good accuracy on short time scales for
109 source regions with close proximity to the receptor, but this approach has limitations in
110 determining contributions from distant sources to BC in the mid- and upper-troposphere that
111 could contribute significantly to the total column burden but less to BC deposition and boundary-
112 layer concentrations. Using the adjoint of the GEOS-Chem global chemical transport model,
113 Kopacz et al. (2011) attempted to identify the originating locations of BC arriving at five glacier
114 sites (i.e., five model grid-cells as the receptors) in the HTP for year 2001. This method can
115 provide a global distribution of emissions that directly contribute to BC concentrations at

receptor locations. Note that the adjoint model results are not source attributions but rather the source-receptor sensitivities, which can be interpreted as the effectiveness of incremental changes to existing emissions in affecting BC at receptor locations. While the adjoint approach has the advantage of not predefining source regions, it does require performing separate simulations for each of the defined receptor regions.

In this study, we use an aerosol-climate model with a newly developed explicit source tagging approach (Wang et al., 2014) to produce a detailed characterization of the fate of BC emitted from various geographical regions and sectors (e.g., fossil fuel, biofuel and biomass burning emissions) and transport pathways to the HTP. In contrast to the back-trajectory and the adjoint approaches, the direct tagging method has the flexibility to do source attribution of BC mass mixing ratio at any model layer and the surface dry and/or wet deposition within a single simulation for any receptor regions. Section 2 describes the aerosol-climate model and the tagging method used in this study. Section 3 presents an evaluation of modeled BC surface concentrations and seasonal snow cover over the HTP region. The transport pathways and source attribution results are presented in Sect. 4. The radiative effects of BC in the atmosphere and of both BC and mineral dust in snow are compared in Sect. 5, followed by the summary and conclusions in Sect. 6.

## 2 Model Configuration and Experimental Design

### 2.1 The CAM5 model and the source-tagging method

We use the Community Atmosphere Model Version 5 (CAM5; Neale et al., 2012), which is the atmospheric component of the Community Earth System Model version 1 (CESM1) (Hurrell et al., 2013). It includes relatively comprehensive representations of aerosols and clouds, and

mechanisms for their interactions with each other and with climate (Gettelman et al., 2010; Liu et al., 2012). CAM5 employs a modal aerosol module (MAM) to represent aerosols in multiple log-normally distributed modes, with internal mixing assumed for aerosol species within each individual mode, including a 3-mode standard representation (MAM3) and a more complex 7-mode representation (MAM7). The major difference between MAM3 and MAM7 related to carbonaceous aerosols lies in the treatment of aging. In MAM3, BC and primary organic matter (POM) particles are emitted into the accumulation mode that also contains highly hygroscopic species such as sulfate and sea-salt, while in MAM7 BC and POM are emitted into a primary carbon mode, which contains no other species. BC is hydrophobic upon emission, and thus the hygroscopicity of the primary-carbon-mode particles depends on the assumed hygroscopicity for POM. As more hygroscopic species (e.g., $H_2SO_4$ and $NH_3$) condense onto the primary-carbon-mode particles, the particles are become more hygroscopic and are gradually transferred into the MAM7 accumulation mode. The rate of transfer is controlled by uncertain aging parameters, and the availability of gas precursors (Liu et al. 2012). In the accumulation mode of both MAM3 and MAM7, BC is internally mixed with other more hygroscopic species and is thus subject to wet scavenging and removal processes. During the transport from sources to remote regions, aerosols are removed too efficiently in the default CAM5 (Liu et al., 2012). Recently, H. Wang et al. (2013) revised some key processes associated with aerosol wet removal and convective transport, which significantly improved the vertical distribution of aerosols and their transport to remote regions such as the Arctic.

To better characterize the sensitivity of BC spatial distributions to emission uncertainties, Wang et al. (2014) implemented a direct source tagging method in CAM5, whereby BC emitted from a number of independent source regions and/or sectors can be tagged and explicitly tracked

within a single model simulation. This approach provides the quantitative characterization of source-receptor relationships for BC in any receptor region without perturbing emissions from individual BC source regions or sectors. In this study, we apply the BC tagging technique to the accumulation-mode BC in the MAM3 treatment. BC particles emitted from sixteen geographical BC source regions and two emissions sectors (i.e., biomass burning & biofuel emissions and fossil fuel emissions) in each of the regions are tagged and explicitly tracked. Instead of using the global emissions from all sectors for the original one BC mass mixing ratio variable, the thirty two regional/sectoral emissions provide sources to the respective tagged BC mass mixing ratio variables that are all added to the accumulation mode, including both interstitial and cloud-borne states. All physical and dynamic tendencies (e.g., transport, dry and wet removal) are calculated explicitly for the tagged BC mass mixing ratio variables in the same way as the original single BC mass mixing ratio. Also, when aerosol optical properties are calculated, all of the tagged BC mass mixing ratios contribute to the volume-mean refractive index of the accumulation mode that is used in the radiation calculation.

In addition to the free-running mode, CAM5 can also be configured in an offline mode, in which temperature, wind, surface fluxes (heat, moisture, and momentum), and pressure are constrained to agree closely with observations, while clouds and aerosol are allowed to evolve freely (Rasch et al., 1997; Lamarque et al., 2012; Ma et al., 2013). In this study, we run the CAM5 model in the offline mode with the direct BC source tagging capability, including the improved representation of convective transport and wet removal of aerosols. We use the NASA Modern Era Retrospective-Analysis for Research and Applications (MERRA) reanalysis dataset (Rienecker et al., 2011), using a horizontal resolution of 1.9° × 2.5° and 56 vertical levels. The goal is to characterize the fate of BC emitted from various geographical regions and sectors, their

transport pathways to the HTP, and their radiative forcing with seasonal variations. The simulation is performed for year 2001 with prescribed sea surface temperatures.

### 2.2 BC source regions and sectors

BC emission datasets have large uncertainties (e.g., Bond et al., 2013), and there are different inventories available for climate modeling. We use the present-day (i.e., year 2000) monthly mean emission inventories for BC provided by Lamarque et al. (2010). They were built for the climate model simulations in the Coupled Model Intercomparison Project Phase 5 (CMIP5) (Taylor et al., 2012) performed for the fifth assessment report (AR5) of the Intergovernmental Panel on Climate Change (IPCC). The AR5 BC emissions being used in our CAM5 simulation include monthly varying elevated open fire emissions (injection altitude up to 6 km), and yearly constant surface emissions from shipping and from six sectors over land: agricultural waste burning, domestic, energy, industry, transportation, and waste treatment. These surface BC emissions sectors do not distinguished between biofuel and fossil fuel combustion. To prepare for the BC source sector tagging, we divide the total surface emissions into two broader sectors, biofuel and fossil fuel, by using the ratio of biofuel to biofuel plus fossil fuel at each model grid provided by Dentener et al. (2006). We then combine the biomass burning (open fire) emissions and surface biofuel emissions, hereafter, referred to as BB (biofuel and biomass) sector. The shipping emissions are combined with the fossil fuel emissions over land to form the FF (fossil fuel) sector. Note that emissions in the BB sector have seasonal variations (associated with the open fire emissions) but the FF sector emissions used in this study have no seasonal variation at all.

The sixteen geographical BC source regions (Fig. 1a) are defined using the definition of source/receptor regions by Work Plan (WP 2.1) of the Task Force on Hemispheric Transport of

208 Air Pollution (http://iek8wikis.iek.fz-juelich.de/HTAPWiki/WP2.1). They are ARC (Arctic),
209 NAM (North America), CAM (Central America), SAM (South America), EUR (Europe), NAF
210 (North Africa), SAF (South Africa), MDE (Middle East), CAS (Central Asia), SAS (South Asia),
211 EAS (East Asia), SEA (South East Asia), PAN (Pacific, Australia and New Zealand), RBU
212 (Russia, Belarus and Ukraine), HTP (Himalayas and Tibetan Plateau) and ROW (Rest of World).

213 Figure 1b and Table S1 in the Supplement summarize the fractional contributions of BC
214 emissions from the different source regions and sectors. The global annual mean BC emission
215 rate is 7.78 Tg $yr^{-1}$, with 56.2% (sum of the red bars) from BB emissions (33.6% from fires and
216 22.6% from biofuel) and 43.8% (sum of the blue bars) from FF emissions. The two largest
217 contributors are BB emissions from SAF (about 20%) and FF emissions from EAS (about 15%),
218 followed by BB emissions from SEA (7.7%), EAS (6.4%), SAS (6.2%) and SAM (5.7%), and
219 EUR FF (6.4%) emissions. The geographical distributions of BC annual mean emission fluxes
220 from BB and FF sectors for year 2000 are shown in Fig. S1 (in Supplement). The global annual
221 and seasonal mean lifetime of BC emitted from the tagged source regions and sectors are
222 summarized in Table S2. On the globe average, BB BC has a longer lifetime than FF BC in all
223 seasons, especially in boreal winter (6.9 vs. 3.1 day), due in part to higher open-fire emissions (in
224 the BB sector) during local dry seasons. Another reason is that open-fire emissions have initial
225 injection heights of up to 6 km, resulting in less removal below 6 km. The availability of co-
226 emitted hygroscopic species that are internally mixed with BC in the accumulation mode of the
227 MAM3 aerosol treatment also impacts the scavenging and wet removal rate of BC. This also in
228 part explains the variability of BC lifetime among the different source regions and sectors.
229 Regarding the seasonal cycle, BC emitted from the major source regions (e.g., SAF, EAS, SEA,

SAS) has substantially lower lifetime in summer (JJA) than in the other seasons, likely due to relatively strong removal by the summer monsoon precipitation.

We use two metrics for quantifying source-receptor relationships and the sensitivity of BC in a receptor region to various sources following Wang et al. (2014), but we extend them to treat BB and FF sectors separately.

1) The fractional contribution of BB and FF emissions from source region *i* to a BC property in the receptor region (HTP), $C_i^{BB}$ or $C_i^{FF}$, is defined as

$$C_i^{BB} = \frac{A_i^{BB}}{\sum_{i=1}^{N}(A_i^{BB}+A_i^{FF})}, C_i^{FF} = \frac{A_i^{FF}}{\sum_{i=1}^{N}(A_i^{BB}+A_i^{FF})} \quad (1)$$

Where $A_i^{BB}$ *and* $A_i^{FF}$ are a BC property (e.g., mass mixing ratio, column burden, or deposition flux) in/over the receptor region resulting from BB and FF emissions, respectively, in source region *i*. The summation $\sum_{i=1}^{N}(A_i^{BB} + A_i^{FF})$ represents the total BC from all source regions (N = 16 in this study) and sectors (BB and FF). Note that for BC properties such as column burden, surface mixing ratio, and deposition flux, the tagging method in CAM5 explicitly calculates how much is due to emissions from each source region and sector.

2) Efficiency of BB and FF emissions from source region *i* in changing BC in a receptor region is defined as

$$S_i^{BB} = \frac{C_i^{BB}}{\left[\frac{E_i^{BB}}{\sum_{i=1}^{N}(E_i^{BB}+E_i^{FF})}\right]}, S_i^{FF} = \frac{C_i^{FF}}{\left[\frac{E_i^{FF}}{\sum_{i=1}^{N}(E_i^{BB}+E_i^{FF})}\right]} \quad (2)$$

Where $C_i^{BB}$ *and* $C_i^{FF}$ are the fractional contribution defined in Eq. (1), and $E_i^{BB}$ *and* $E_i^{FF}$ are the total BB and FF emission rates, respectively, in source region *i*. The summation $\sum_{i=1}^{N}(E_i^{BB} + E_i^{FF})$ in Eq. (2) represents the global total emission rate. The efficiency metric $S_i^{BB}$ *or* $S_i^{FF}$ also characterizes the sensitivity of aerosol properties in the receptor region to per unit (BB or FF)

emissions in the source region. This metric is of more interest to policy makers for the purpose of mitigation action, which is not the focus of this study but is worth mentioning.

## 3 Model evaluation against available observations

The CAM5 model has been evaluated in detail from different perspectives with available observations such as aerosol mass concentration, aerosol number concentration and size distribution, aerosol optical properties, cloud properties, aerosol deposition and BC in snow over various regions in previous studies (Liu et al., 2012; H. Wang et al., 2013; Ma et al., 2013; Jiao et al., 2014; Lee et al., 2013; Qian et al., 2014). Because of the complex topography and meteorology of the HTP and the relatively coarse resolution of global model, further model evaluation focusing on the HTP region is critical. Here we use near-surface atmospheric BC concentrations measured at a few HTP sites and the snow cover fraction retrieved from satellite to evaluate the CAM5 performance in the HTP.

### 3.1 Atmospheric BC surface concentration

There are seven remote sites that have surface measurements of seasonal BC aerosol concentrations available. The locations and elevations of the sites and the sampling time periods and observation methods are described in Table 1. Figure 2 shows the comparison of seasonal mean BC concentrations between observations and CAM5 results. Note that model results represent mean concentrations in the grid box that the sampling sites reside in and at the grid-mean elevation, which could deviate significantly from the sampling point near complex terrain. All sites have non-negligible amounts of BC in the near-surface air. The error bars indicate the intra-seasonal and inter-annual variations if multi-year data were used for given season and site. However, the uncertainties of observed BC surface concentrations mainly originate from the

large discrepancies between different measurement methods, the mixing of BC with other components (e.g., organic carbon and mineral dust) in the aerosol samples, and the sampling time and location (Bond et al., 2013; Petzold et al., 2013). BC surface concentrations over the various sites show strong seasonal variations, which are reasonably captured by the model. The modeled magnitude of BC concentrations has a good agreement with observations at some sites (e.g., Fig. 2b, d, g), but the model clearly overestimates BC at the Muztagh Ata site (Fig. 2a) and underestimates at the Lulang site (Fig. 2e). The large underestimation (about 1000 m; see Table 1) of the Muztagh Ata site elevation in the model, determined by the model grid resolution, could largely explain the overestimation of BC since BC concentrations have sharp decreases with height in this region. At the sites over southern HTP (i.e., Hanle, Manora Peak, NCO-P, Lulang and NCOS), the BC surface concentrations in the summer (JJA) are lower, mainly due to wet scavenging by more frequent precipitation and partly due to the minimal emissions from domestic heating and wildfires over Himalaya foothills and Indo-Gangetic Plains (IGP) during the Indian summer monsoon season (Marinoni et al., 2010, 2013). Among all these sites, the largest BC surface concentrations occur at the Manora Peak site that is closer to the major sources in South Asia, especially in the winter (DJF) when the model underestimates the concentrations by about 50%. The high concentrations in winter at Manora Peak is mainly due to the dry winter monsoon conditions and increased transport of emissions from regional biomass burning, agricultural waste and wood fuel burning from the IGP (e.g., Ram et al., 2010; Moorthy et al., 2013). The BC surface concentrations peak in the springtime (MAM) at Hanle, NCO-P, Lulang and NCOS sites. This might be related to an increase in BB and/or FF emissions in the Indian Subcontinent, along with the higher regional boundary-layer top over the IGP during the springtime that may favor the transport of particles from the surface up to higher altitudes (e.g.,

297 Marinoni et al., 2010, 2013). Moreover, a long-range transport of pollution emitted from distant
298 regions like the Middle East, North Africa or Europe (Marinoni et al., 2010) could further
299 contribute to BC variability over the South Himalayas, which will also be examined in this study.
300 Part of the discrepancies between observations and model results can be attributed to the inherent
301 difficulty in simulating the cloud/precipitation fields over the complex topography and
302 subsequent wet removal of aerosols during the transport, but emission uncertainties (e.g., Bond
303 et al., 2013) might play a primary role.

304 **3.2 Snow cover fraction**

305 It is important to evaluate the performance of model in simulating seasonal snow over this region
306 in order to assess the importance of BC-in-snow effect. Figure 3 shows the CAM5 simulated
307 seasonal and annual mean snow cover fraction (SCF) during year 2001, in comparison to
308 observed mean SCF, derived from the Moderate Resolution Imaging Spectrometer (MODIS)
309 (Hall et al., 2006) monthly mean of daily products at 0.05 degree resolution. For a better
310 comparison, the MODIS monthly mean SCFs are mapped to the CAM5 grid. The summer (JJA)
311 season only includes July and August for both CAM5 and MODIS due to missing MODIS data
312 in June 2001. To illustrate whether year 2001 can represent the average condition in terms of
313 SCF, the MODIS SCF climatology (2000-2013) is also plotted. The overall SCF in HTP has very
314 small difference between climatology and year 2001 in all seasons except for JJA, when SCF is
315 notably higher over northwest Plateau for the climatology that included June SCF in the average.
316 On average, SCF is about 5% (absolute amount) higher in June than in July and August. Over the
317 52 HTP grid cells, the CAM5 SCF is highly correlated spatially with that of MODIS (for both
318 2001 and 2000-2013) with the statistical confidence level greater than 99%, except for summer
319 (JJA) when the linear correlation is significant only at 80% level.

There are strong spatial and seasonal variations in SCF due to the complex terrain and seasonal variation in snowfall and melting. The SCF over the entire HTP reaches the maximum in the winter (DJF), while decreases to almost none (less than 5%) in July and August. Snow covers the western and southeastern Plateau during the transition seasons (MAM and SON). The CAM5 simulation shows a good agreement with MODIS in the annual mean (ANN) SCF and the strong seasonality. The most persistent snow cover at the southern and western edges of the HTP and the relatively less persistent in the HTP interior are captured by the CAM5 model. The performance of the CAM5 has been improved, in comparison to its earlier version (CAM3) that remarkably overestimated the SCF especially over the HTP interior (Qian et al., 2011), although the CAM5 still significantly overestimates the SCF in the western Plateau in DJF and MAM and underestimates it in JJA. The CAM3 model used by Qian et al. (2011) overestimates SCF by up to a factor of 2 during the cold season (November to April). The CAM3 spring (MAM) mean SCF is greater than 35%, while the CAM5 spring mean (21%) in the present study is in good agreement with the MODIS spring SCF (18±5%).

Although we believe that the CAM5 SCF biases are qualitatively robust, it is worth noting that the MODIS products have uncertainties as well. Pu et al. (2007) evaluated the MODIS SCF products over the HTP against ground-based snow observations and showed that total error in MODIS SCF products over the HTP is about 10%. However, their analysis based on MODIS eight-day snow-cover composite gave a significantly higher SCF (more than 10%) than the one we show here using daily products, especially, in winter and early spring. Interestingly, based on a different source of observation, Qin et al. (2006) found that snow covers about 59% of the Tibetan Plateau in winter, which is comparable to the mean SCF (50%) in our

342 CAM5 simulation. Nonetheless, we keep this discrepancy in mind when interpreting the
343 wintertime BC-in-snow radiative forcing that suffers the most from such potential SCF bias.
344
345 **4 Modeled transport pathways and source attribution of BC in the HTP**
346 **4.1 Transport pathways**
347 The direct source tagging method can clearly characterize the three-dimensional transport
348 pathways of BC emitted from various source regions and sectors to the HTP receptor region.
349 General circulation patterns over the HTP and surroundings are typically affected by mid-latitude
350 westerlies in the winter and Asian monsoon in the summer, including the South Asian summer
351 monsoon and East Asian summer monsoon (Xu et al., 2009; Yao et al., 2012; Wu et al., 2012;
352 also see Fig. S2).
353 Figure 4 illustrates circulation patterns over HTP and BC transport pathways from six
354 major source regions to the HTP in the winter (DJF) and summer (JJA). (See similar plots in
355 Figs. S3−S5 for other tagged source regions.) In the winter, the strong surface cooling over the
356 HTP leads to subsidence/divergence and the formation of an enhanced local circulation cell,
357 while in the summer air converges toward the HTP from the surroundings, particularly from the
358 South Asia, due to the ascending of strongly heated air over the HTP (e.g., Wu et al., 2012), as
359 also indicated by the arrows in the vertical cross-sections in Fig. 4. In the winter, the subtropical
360 westerlies extend to about 10°N in mid-/upper troposphere and 20°N near surface, and the
361 tropical easterlies are weak (see the white contours of latitude-height cross-section panels in Fig.
362 4). The circulation patterns near the HTP change dramatically during the summer monsoon
363 season. The reversal of surface wind regime in the tropics (e.g., Arabian Sea, Bay of Bengal, and

South China Sea) is characteristic of the Asian summer monsoon climate (see Fig. S2e, g). The subtropical westerlies recede to north of 30°N and the center of the westerly jet shifts to about 40°N in JJA (from about 30°N in DJF). The strong easterlies characterize the upper troposphere of tropical region (south of HTP), while the southwesterly flow prevails in the lower troposphere (white contours of latitude-height cross-section panels in Fig. 4). The prevailing winds during the transition seasons (MAM and SON) between DJF and JJA are still westerlies (Fig. S2b, d).

The circulation patterns determine the transport of BC around the HTP region. However, the variations of spatial distributions of BC emitted from the different source regions and in different seasons could be due to the differences in source location and strength, wet removal rate and lifting. Note that although we combined BC emitted from BB and FF sections to characterize transport pathways in Fig. 4, only BC emissions from BB sector have seasonal variations in the emission inventory we use.

The HTP region is surrounded by two major BC source regions, SAS and EAS (Fig. 1a), which potentially have great impact on BC in the HTP (e.g., Menon et al., 2010; Bond et al., 2007; Ohara et al., 2007; Xu et al., 2009; Kopacz et al., 2011; Lu et al., 2012). BC emissions from SAS are dominated by the BB sector, and by FF sector from EAS (Fig. 1b). As shown in Fig. 4, in the winter, a significant amount of BC from SAS can be transported to the eastern Plateau by the strong westerlies under the dry winter monsoon conditions. During the South Asian summer monsoon BC from SAS is effectively removed by the local abundant precipitation, as indicated by the low lifetime in summer (Table S2), but can still affect large area in the southwest of the HTP. However, BC from EAS can be uplifted higher and transported more to the Northeast Plateau in the summer monsoon season than in the winter. Along the wintertime westerlies, BC from upwind source regions (e.g., EUR, NAF, SAF, MDE, and CAS)

can easily move to the HTP, while the HTP local emissions are transported far away (Fig. 4). BC originating from the distant sources such as SAF and MDE reaches up high (to 300hPa) in the HTP. In the summer, continental deep convection can loft BC into higher altitudes where it can be transported to the HTP along the relatively weaker westerlies from upwind source regions (e.g., EUR, RBU, MDE, and CAS). However, BC from distant low-latitude source regions such as SAF barely reaches the HTP region due to weak emissions but strong removal along the transport pathways to the HTP during the summer monsoon season.

### 4.2 Seasonal variation of BC in the HTP

BC concentrations in the HTP have strong dependence on season and location. Figure 5 shows the annual mean and seasonal variations of BC column burden and deposition rate over the HTP and five sub-regions. The seasonal variation of the ratio of wet to total BC deposition is superimposed. The Central Plateau is the cleanest region during all seasons, compared to other sub-regions in the HTP (Fig. 5e). Both BC column burden and deposition rate from the BB sector peak in MAM over the HTP, mostly in the Himalayas and Southeast Plateau region. The FF BC burden in the HTP peaks in the summer mainly due to the seasonal maximum over Northwest and Northeast Plateaus. However, BC wet removal rate over the Northwest Plateau is at minimum in the summer, as opposed to the summer maximum in other sub-regions and the entire HTP region. For Himalayas, Southeast and Central Plateau, the seasonal variation (i.e., maximum in MAM followed by a sharp decrease to JJA) of BB and FF column burden (Fig. 5c, d and e) is similar to the variation of observed surface concentrations at sites located in these sub-regions (Fig. 2b, d, e and f). In the Himalayas and Southeast Plateau, the ratio of regional mean BC column burden to deposition rate (Fig. 5c and d), indicator of removal time scale or lifetime, is the smallest (less than 1 day) during the Asian summer monsoon (JJA) due to the

efficient wet scavenging of BC by abundant precipitation. In Northwest and Northeast Plateau, the BC column burden increases from DJF to JJA and reaches the maximum in JJA, and then decreases in SON (Fig. 5b and f), partly due to the peak contribution of EAS and CAS emissions in JJA. This trend is also similar to that in the observed surface concentrations (Fig. 2a and g). The deposition rate follows the same seasonal variation of column burden over the Northeast Plateau, while the deposition has a minimum in JJA over the Northwest Plateau when the column burden is at maximum likely due to the less efficient wet removal in this region (Fig. 5b and f).

The annual mean BC column burden over the HTP has almost the same contributions from BB and FF emission origins, with BB dominating in DJF and MAM and FF in JJA. In the Himalayas, BC is predominantly from BB sector for all seasons (Fig. 5c). In the Southeast and Central Plateaus, the dominant source sector is BB in DJF and MAM, but FF dominates in JJA. The dominant source sector over the Northwest and Northeast Plateaus is always FF, especially in the summer. We need to analyze the source-receptor relationships in order to quantify the roles of BB and FF emissions from the various source regions in determining BC over the HTP and the sub-regions.

### 4.3 BC source-receptor relationships

Previous studies (e.g., Xu et al., 2009; Kopacz et al., 2011) have shown that BC and its source-receptor relationships vary significantly with season and location in the HTP. We intend to quantify source contributions to BC at different locations of the HTP and in different seasons. Our analysis also shows that the relative contributions to BC from different source regions and sectors depend on season and location in the HTP. As shown in Fig. 6, the largest contribution to the annual mean BC burden and surface deposition for the entire HTP region is from BB

emissions from SAS, followed by FF emissions from SAS and then the FF from EAS. The same roles hold for all the seasonal means except for the summer (JJA) when the EAS FF becomes more important for BC column burden in the HTP and, to a lesser extent, for deposition.

The SAS emissions account for 50% of the annual mean burden over the HTP, including 33% from BB and 17% from FF. The other 50% is mostly from the EAS (5% BB and 14% FF), HTP (6% BB and 6% FF), CAS FF (4%), MDE FF (4%) and SAF BB (3%). The source attribution for annual mean BC deposition for the entire HTP is similar, but SAS contributes even more to BC deposition than to the column burden. Although RBU has a lower contribution to the annual mean BC in the HTP than the six regions shown in Fig. 6, its contribution to the JJA mean, especially at some locations, is quite substantial (included in the black bar) and even more important than some of the six regions in Fig. 6, as discussed in detail below.

BC annual mean burden over the HTP has nearly equal contributions from BB and FF emissions. However, contribution by BB emissions, mainly from SAS, is larger than from FF sector in DJF and MAM. In the summer (JJA), the largest contribution (about 29%) to HTP BC is from EAS FF emissions. This is partly due to the change of circulation patterns (Fig. 4) and effective wet removal of SAS BB emissions. Note that EAS FF emissions are much larger than FF emissions from any other of the source regions, and are more than twice the EAS BB emissions.

For BC in the five finer receptor regions of interest (as defined in Fig. 5g), SAS BB and FF have the largest contribution to BC in Himalayas and Central Plateau, while EAS FF and BB contribute the most to Northeast Plateau in all seasons and Southeast Plateau in the summer.

453 Central Asia and Middle East FF emissions have relatively more important contribution to BC
454 reaching Northwest Plateau, especially in the summer.

455 For the Northwest Plateau (Fig. 6b), the prevailing winds in this sub-region are westerly
456 throughout the year (Fig. S2; Cao et al., 2009; Xu et al., 2009), so the important source regions
457 ought to locate at the west of HTP (e.g., MDE, EUR, and parts of SAS and RBU in Fig. 1a). SAS
458 emissions are still the dominant source for the annual BC burden in this sub-region (17% from
459 BB and 14% from FF), followed by HTP local emissions (9% from BB and 13% from FF), CAS
460 (2% from BB and 14% from FF), MDE FF (8%) and EAS FF (7%). BC emissions from SAS are
461 the dominant source in DJF, MAM and SON. CAS becomes the dominant source region (5%
462 from BB and 26% from FF) in JJA, even though CAS is not a significant emission source region
463 on a global basis (Fig. 1b). BC emitted from MDE is predominantly in the FF sector throughout
464 the year. Emissions from the rest of the tagged sources (in addition to the top six) become more
465 significant in this sub-region (black color in Fig. 6b), mostly from EUR and RBU through long-
466 range transport (Fig. S3). The source attribution for BC deposition in this sub-region is similar to
467 that of the column burden, but BC emitted from SAS and MDE appears to be more efficient in
468 deposition except for the JJA season when BC from EAS contributes more to deposition than to
469 column burden.

470 The Himalayas sub-region located along the southern edge of the HTP is in close
471 proximity to the SAS. Thus emissions from SAS are absolutely the dominant source for BC in
472 Himalayas throughout the year. This sub-region receives more BC from BB sector than FF
473 because BC emissions in SAS are mainly in the BB sector, especially in MAM season (Fig. 1b
474 and Fig. S6). For the annual mean burden, BC from SAS contributes 81% (54% from BB and
475 27% from FF), followed by HTP local emissions (6% from BB and 3% from FF). It is worth

476 noting that SAF BB emissions contribute about 10% to burden in DJF through a long-range
477 transport. BC deposition in this sub-region also predominantly originates from SAS, which is
478 consistent with previous studies by Ming et al. (2008) and Kopacz et al. (2011).

479 For the Southeast Plateau (Fig. 6d), the BC source contribution profile is similar to that of
480 Himalayas during DJF and MAM season, in which SAS is still the dominant source, especially
481 in MAM (74% contribution to column burden, including 53% from BB and 21% from FF),
482 although the contribution from EAS is larger here than for the Himalayas. As also pointed by
483 Ramanathan et al. (2007), BC over the SAS can be transported to the Southeast Plateau by the
484 southern branch of the westerlies during the winter and spring. However, the BC source
485 contribution profile changes dramatically during the summer when emissions in EAS become the
486 dominant source to this sub-region (68% to column burden, including 23% from BB and 45%
487 from FF). Kopacz et al. (2011) also found that the BC from south-eastern China is the dominant
488 contributor to the Southeast Plateau in July. For the annual mean burden in this sub-region, SAS
489 is still the dominant contributor (40% from BB and 17% from FF), followed by EAS (8% from
490 BB and 15% from FF), HTP (6% from BB and 6% from FF). BC originating from EAS
491 contributes more to deposition than to burden in this sub-region.

492 For the Central Plateau (Fig. 6e), source attribution profiles for annual and seasonal BC
493 are very similar to those of the entire HTP region with SAS being the dominant source region
494 throughout the year except that EAS has comparable contributions in JJA. Ming et al. (2010)
495 pointed out that pollutants from the Indo-Gangetic Basin could be transported to the Central
496 Plateau by both the summer monsoon and the westerlies. Xia et al. (2011) also found that the
497 substantial regional atmospheric brown haze from the nearby regions of SAS is the main source

for the background aerosols in the Central Plateau based on sunphotometer and satellite observations.

Compared to the other sub-regions, the Northeast Plateau receives the largest contribution of BC from EAS throughout the year (50% to annual mean burden, including 12% from BB and 38% from FF; see Fig. 6f), especially in JJA (17% from BB and 49% from FF). The EAS FF sector contribution and the magnitude of burden (Fig. 5f) over the Northeast Plateau have strong seasonal variations, mostly due to variations in meteorology because the FF emissions in our simulation do not vary seasonally. Kopacz et al. (2011) indicate that the primary contribution to BC over the Northeast Plateau is from western China during January and April (transported by mid-tropospheric westerlies), and from central-eastern China during July and October (transported by boundary layer flow). Other main contributions to BC burden over the Northeast Plateau include 13% from SAS and 10% from HTP local emissions. Similar to the Northwest Plateau, some other upwind source regions (e.g., CAS, MDE, RBU and EUR) have a significant contribution to the Northeast sub-region as well.

### 4.4 Seasonal variation of HTP BC sensitivity

Following Wang et al. (2014), we defined the "efficiency" metric in Sect. 2.2 to quantify the sensitivity of BC response to absolute change (e.g., per unit perturbation) of emissions in different source regions. This metric has the value of 1 if the entire globe is treated as a single source region, so we may assume the global mean efficiency of 1 as a reference to measure the sensitivity to perturbation from different source regions/sectors.

Figure 7 shows efficiencies of tagged sources in affecting the BC seasonal and annual mean column burden and deposition in the HTP and five sub-regions (as defined in Fig. 5g). BC

in the same receptor regions is generally most sensitive to change in local emissions, regardless of seasons, emission sectors and locations of receptor regions. Among all the source regions, although the HTP local (FF+BB) emissions only contribute about 10%, BC in the HTP is extremely sensitive to changes in the emissions within HTP. In addition to the local emissions, BC in the HTP is also sensitive to emissions in neighboring source regions (e.g., SAS and CAS) and emissions from distant sources such as MDE. Not only does the SAS have large contribution to BC burden and deposition over the HTP, as well as most of the sub-regions except for the Northeast Plateau (receptor V), but also the efficiencies for SAS emissions are high for almost all of the sub-regions especially the Himalayas (receptor II). BC in the Northeast Plateau (receptor V) is quite sensitive to EAS emissions in all seasons, while BC in the Southeast Plateau is sensitive to EAS emissions in JJA and SON. Although BC emissions from MDE and CAS are weak (Fig. 1b) and their contributions to the HTP are relatively low, their efficiencies are high. BC over Northwest Plateau (receptor I) and Central Plateau (receptor IV) is extremely sensitive to emissions from CAS in JJA. These source-receptor relationships of sensitivity will provide useful information for policymakers to improve the effective mitigation road map in order to potentially slow down the glacier retreat in the HTP region.

## 5 Radiative forcing

The BC-in-snow effect can be quantified using the online calculation of radiative forcing in the SNICAR (Snow, Ice, and Aerosol Radiative) model (Flanner et al., 2007) coupled to CAM5, and then compared to airborne BC radiative forcing. Figure 8 shows seasonal and annual mean BC all-sky shortwave direct radiative forcing (DRF) at the surface (dimming) and the top of the

atmosphere (TOA), and the BC-in-snow radiative forcing (darkening) averaged over the entire HTP and the five sub-regions (as defined in Fig. 5g). Note that the BC-in-snow forcing is averaged over all model grids in the area (i.e., zero enters the calculation for any grid when snow is not present). The radiative forcing of BC (and dust) in snow is small in JJA and SON due to a lack of snow cover (Fig. 3). The forcing maximum occurs during the spring melt (MAM) when the insolation is rather intense and BC accumulates at the surface of the snowpack as the snow melts (Conway et al., 1996; Flanner et al., 2007, 2009), and when the snow-albedo feedback is strongest (Hall and Qu, 2006). This strong seasonal variation also explains why the coefficient of variation (i.e., the ratio of the SD to the mean) is greater than 1 for the annual mean BC-in-snow forcing over the entire HTP and all sub-regions. The seasonal variations of airborne BC DRF at the TOA and surface are consistent with that of the BC column burden (Fig. 5). For the entire HTP (Fig. 8a1), the annual mean surface radiative forcing due to BC in snow (0.42 W $m^{-2}$) exceeds the BC dimming effect at the surface (-0.3 W $m^{-2}$). The annual mean BC-in-snow forcing is even higher over the Northwest Plateau (Fig. 8b1) and Himalayas (Fig. 8c1), and far exceeds the other forcings in the same sub-regions, although the BC-in-snow effect may be overestimated due to the potential positive bias in snow cover fraction in our simulation (Fig. 3). The annual mean BC surface dimming exceeds the BC-in-snow effect in the Southeast (Fig. 8d1), Central (Fig. 8e1) and Northeast Plateau (Fig. 8f1). The minima of all BC-related forcings appear in the Central Plateau where the BC burden and deposition are the lowest among all the sub-regions (Fig. 5), and the SCF is very small (Fig. 3).

We have also calculated an approximate source attribution for the BC-in-snow radiative forcing over the HTP and its sub-regions, using the tagged-source BC deposition, which is simply assumed to be linearly proportional to BC-in-snow radiative forcing. The SCF is taken

565 into account in the calculation (i.e., the deposition at each model grid is multiplied by SCF when
566 calculating the area-average deposition). Overall, despite small quantitative differences, the
567 source contributions to BC-in-snow forcing are similar to those for BC deposition (Fig. 6). The
568 SAS BB emissions contribute the most to annual mean forcing over the HTP and sub-regions
569 except for the Northeast Plateau that is mostly contributed by EAS FF emissions. During the
570 winter and spring seasons over Northwest Plateau and Himalayas, when and where the forcing is
571 the largest, SAS (especially the BB sector) is the major contributor.

572 Dust is a major contributor to the total aerosol burden over the HTP (e.g., Zhang et al.,
573 2001). Although we don't focus on other snow impurities such as mineral dust, it is worth noting
574 that dust-in-snow radiative forcing has been considered in our model simulation and it could be
575 an important forcing agent. We also plotted dust-in-snow forcing over the HTP and sub-regions
576 in Fig. 8 (along with the BC-induced forcings). The annual mean dust-in-snow forcing (0.33 W
577 $m^{-2}$) is comparable to all of the other forcings over the HTP, especially in the springtime when
578 dust outbreaks and can be transported to the HTP from the surrounding sources such as
579 Taklimakan and Gobi deserts (Liu et al., 2008). The annual mean dust-in-snow forcing is as large
580 as 0.99 and 0.59 W $m^{-2}$ in the Northwest and Northeast Plateau, respectively (Fig. 8b1 and f1),
581 which is in close proximity to the Taklimakan Desert (Huang et al., 2007; Chen et al., 2013), but
582 negligibly small in the Southeast Plateau and Central Plateau. In the winter, the dominant dust in
583 snow effect over Northeast Plateau is consistent with the recent observations. Huang et al. (2011),
584 X. Wang et al. (2013) and Zhang et al. (2013) found that insoluble light-absorbing particles in
585 snow are dominated by local soil and desert dust in the Qilian Mountain (Northeast Plateau).

586 Both snow cover fraction (SCF) and mass concentration of snow impurities affect the
587 calculation of radiative forcing in snow. We have evaluated the model estimation of SCF in

588 different seasons (Fig. 3). We have also compared BC concentration and deposition flux from
589 our model results to a recent modeling study by Ménégoz et al. (2014) and to observations in the
590 HTP (Ginot et al., 2014) (Table S3). Bond et al. (2013) pointed out that observations of BC in
591 snow pits or ice cores mostly involve snow/ice samples obtained in the summer and early fall,
592 when almost all grid boxes the sample sites located in are snow free in the HTP. They also
593 indicated that the CAM3 global climate model (Flanner et al., 2009) may be overestimating snow
594 BC concentrations in the HTP, especially in the spring. Our comparison shows that despite a
595 smaller bias than in Ménégoz et al. (2014) the CAM5 model still largely overestimates BC
596 concentrations in snow but underestimates dust concentrations in snow over the HTP. Ménégoz
597 et al. (2014) provided a few possible reasons for the differences between model simulations and
598 observations. Factors such as measurement uncertainties (due to sample treatment and analysis
599 methodology), temporal (inter-annual and seasonal) and spatial variations of BC deposition, and
600 vertical variations of BC in snowpack, can strongly affect the accuracy and representativeness of
601 BC-in-snow measurements for the purpose of evaluating global models. Ming et al. (2013) and
602 Qian et al. (2015) pointed out that BC concentrations in snow and ice samples over HTP tend to
603 decrease with increasing glacier elevations, while global models with coarse grid resolution
604 cannot accurately represent elevation of sampling sites. Often times the difference is significant.
605 Nonetheless, it is likely that positive biases exist in the modeled concentration and radiative
606 forcing of BC and dust in snow.

607 **6 Summary and conclusions**

608 In this study, we employed the CAM5 model with a newly developed source tagging technique,
609 nudged towards the MERRA meteorological reanalysis, to characterize the fate of BC particles
610 emitted from various geographical regions and sectors to the HTP region. In addition, we

611 compare the radiative forcing induced by BC in the atmosphere and in snow over the HTP, as
612 well as forcing induced by dust in snow. Although there are biases in the simulated BC, partly
613 due to the inherent difficulty for coarse-resolution global models to accurately represent transport
614 and wet deposition in this topographically complex region, the CAM5 model simulation shows a
615 reasonable agreement in the seasonal variation of the near-surface airborne BC concentrations
616 with observations over the HTP and surrounding regions. This provides us the confidence to use
617 this modeling framework to characterize BC source-receptor relationships in the HTP. Using
618 very different approaches, Kopacz et al. (2011), Lu et al. (2012) and the present study all show
619 that South Asia and East Asia are the main source regions for BC transported to the HTP, while
620 the magnitude of contributions from each of the source regions varies with season and receptor
621 location. Although all of the three studies can provide quantitative source attributions, a
622 quantitative inter-comparison of the findings is quite difficult, given the differences in the
623 definition of geographical source and receptor regions, emission inventories, time periods for
624 model simulation, and analysis methods. Nevertheless, in addition to quantifying the
625 contributions of source regions, our direct source tagging approach allows us to further break
626 down regional contributions by sectors (i.e., fossil fuel vs. biomass & biofuel) and to characterize
627 the transport pathways of individual regional/sectoral emissions.

628 The explicit source tagging technique enables the characterization of three-dimensional
629 transport pathways of BC to the HTP from different geographical regions and source sectors,
630 which also depends on seasons and the location of the receptor in the HTP. With the IPCC AR5
631 present-day emission inventories, the annual mean BC column burden and surface deposition in
632 the entire HTP region is contributed the most by biomass and biofuel (BB) emissions from South
633 Asia (SAS) (33% and 40%, respectively), followed by fossil fuel (FF) emissions from SAS (17%

634 and 20%, respectively), and then the FF from East Asia (EAS) (14% and 14%, respectively). The
635 same roles hold for all the seasonal means except for the summer when the EAS FF becomes
636 more important. Although BC emissions from the entire EAS source region are much stronger
637 than those from SAS, the concentrated FF BC emissions in central-eastern China are only
638 transported towards the HTP during the East Asian summer monsoon. Thus seasonal prevailing
639 winds are important in determining the seasonal variations in BC transport and source-receptor
640 relationships.

641 Both the annual and seasonal mean BC properties and their source-receptor relationships
642 vary significantly with location in the HTP. For the multiple finer receptor regions of interest,
643 SAS BB and FF have the largest impact on BC in Himalayas and Central Plateau, while EAS FF
644 and BB contribute the most to Northeast Plateau in all seasons and Southeast Plateau in the
645 summer. The Central Asia (CAS) and Middle East (MDE) FF emissions make important
646 contributions to BC over the Northwest Plateau, especially from CAS in JJA.

647 The HTP BC is most sensitive by far to per unit changes in the local emissions, although
648 they only contribute about 10% to the BC burden in the HTP. The SAS region makes large
649 contributions to BC burden and deposition over the HTP and the BC sensitivities to SAS
650 emissions are also high for almost all of the sub-regions of HTP, especially the Himalayas. BC
651 over the Northeast Plateau is quite sensitive to EAS emissions in all seasons, and Southeast
652 Plateau BC is also sensitive to EAS emissions in JJA. Although BC emissions from MDE and
653 CAS are weak and their contribution to the HTP overall is low, their efficiencies are quite high.
654 BC over Northwest Plateau and Central Plateau is extremely sensitive to emissions from CAS in
655 JJA. These source-receptor relationships and sensitivities can be useful to policymakers for

improving the effective mitigation road map in order to potentially slow down the glacier retreat in the HTP region.

The impact of BC on snow and glacier melting can be characterized by the magnitude of radiative forcing. Our calculations show that the annual mean BC-in-snow radiative forcing (0.42 W $m^{-2}$) outweighs BC dimming effect (-0.3 W $m^{-2}$) at the surface over the HTP. In the five sub-regions, the annual mean BC-in-snow forcing ranges from 0.04 W $m^{-2}$ in the Central Plateau to 1.75 W $m^{-2}$ in the Northwest Plateau. We also showed that the annual mean dust-in-snow induced radiative forcing over the HTP can be quite significant (0.33 W $m^{-2}$ for entire the HTP, and 0.99 W $m^{-2}$ for the Northwest Plateau). More importantly, both BC- and dust-in-snow forcing peaks in the spring melting season when the area-average forcing reaches 1.03 and 0.87 W $m^{-2}$, respectively, over the entire HTP, and their combined forcing is more than 8 W $m^{-2}$ over the Northwest Plateau. Such a large forcing is sufficient to cause earlier snow melting and contribute to the acceleration of glacier retreat, although the model is likely to overestimate BC-in-snow forcing due to the possible positive bias of snow cover fraction in the winter and early spring. According to our estimates of the source attribution, the biomass burning and biofuel emissions in South Asia contribute the most to annual mean forcing over the HTP and its sub-regions except for the Northeast Plateau where the largest contribution is from East Asia fossil fuel emissions. During the winter and spring seasons over Northwest Plateau and Himalayas, when and where the forcing is the largest, South Asia (especially the biomass burning and biofuel sector) is the major contributor.

*Acknowledgments.* This research is based on work supported by the U.S. Department of Energy (DOE), Office of Science, Biological and Environmental Research as part of the Earth System Modeling Program. The Pacific Northwest National Laboratory (PNNL) is operated for DOE by Battelle Memorial

Institute under contract DE-AC05-76RLO1830. The CESM project is supported by the National Science Foundation and the DOE Office of Science. R. Zhang acknowledges support from the China Scholarship Fund. J. Huang and Q. Fu acknowledge support from the National Basic Research Program of China (2012CB955303), NSFC grant 41275070 and China 111 project (No. B13045). Computational resources were provided by the National Energy Research Scientific Computing Center (NERSC), a national scientific user facility located at Lawrence Berkeley National Laboratory in Berkeley, California. NERSC is the flagship scientific computing facility for the Office of Science in DOE.

## References

Babu, S. S., Chaubey, J. P., Moorthy, K. K., Gogoi, M. M., Kompalli, S. K., Sreekanth, V., Bagare, S. P., Bhatt, B. C., Gaur, V. K., Prabhu, T. P., and Singh, N. S.: High altitude (~4520 m amsl) measurements of black carbon aerosols over western trans-Himalayas: Seasonal heterogeneity and source apportionment, J. Geophys. Res., 116, D24201, doi:10.1029/2011JD016722, 2011.

Barnett, T. P., Adam, J. C., and Lettenmaier, D. P.: Potential impacts of a warming climate on water availability in snow-dominated regions, Nature, 438, 303–309, doi:10.1038/Nature04141, 2005.

Bolch, T., Kulkarni, A., Kääb, A., Huggel, C., Paul, F., Cogley, J., Frey, H., Kargel, J., Fujita, K., Scheel, M., Bajracharya, S., and Stoffel, M.: The state and fate of Himalayan Glaciers, Science, 336, 310–314, doi:0.1126/science.1215828, 2012.

Bond, T. C., Bhardwaj, E., Dong, R., Jogani, R., Jung, S., Roden, C., Streets, D. G., and Trautmann, N. M.: Historical emissions of black and organic carbon aerosol from energy-related combustion, 1850–2000, Global Biogeochem. Cy., 21, GB2018, doi:10.1029/2006GB002840, 2007.

Bond, T. C., Doherty, S. J., Fahey, D. W., Forster, P. M., Berntsen, T., DeAngelo, B. J., Flanner, M. G., Ghan, S., Kärcher, B., Koch, D., Kinne, S., Kondo, Y., Quinn, P. K., Sarofim, M. C., Schultz, M. G., Schulz, M., Venkataraman, C., Zhang, H., Zhang, S., Bellouin, N., Guttikunda, S. K., Hopke, P. K., Jacobson, M. Z., Kaiser, J. W., Klimont, Z., Lohmann, U., Schwarz, J. P., Shindell, D., Storelvmo, T., Warren, S. G., and Zender, C. S.: Bounding the role of black carbon in the climate system: A scientific assessment, J. Geophys. Res.-Atmos., 118, 5380–5552, doi:10.1002/jgrd.50171, 2013.

Bonasoni, P., Laj, P., Marinoni, A., Sprenger, M., Angelini, F., Arduini, J., Bonaf`e, U., Calzolari, F., Colombo, T., Decesari, S., DiBiagio, C., di Sarra, A. G., Evangelisti, F., Duchi, R., Facchini, MC., Fuzzi, S., Gobbi, G. P., Maione, M., Panday, A., Roccato, F., Sellegri, K., Venzac, H., Verza, GP., Villani, P., Vuillermoz, E., and Cristofanelli, P.: Atmospheric Brown Clouds in the Himalayas: first two years of continuous observations at the Nepal Climate Observatory-Pyramid (5079 m), Atmos. Chem. Phys., 10, 7515–7531, doi:10.5194/acp-10-7515-2010, 2010.

Cao, J. J., Xu, B. Q., He, J. Q., Liu, X. Q., Han, Y. M., Wang, G. H., and Zhu, C. S.: Concentrations, seasonal variations, and transport of carbonaceous aerosol at a remote Mountainous region in western China, Atmos. Environ., 43, 4444–4452, doi:10.1016/j.atmosenv.2009.06.023, 2009.

716 Chen, S., J. Huang, C. Zhao, Y. Qian, L. R. Leung, and B. Yang: Modeling the Transport and Radiative Forcing of
717 Taklimakan Dust over the Tibetan Plateau in Summer, J. Geophys. Res., 118, 797–812,
718 doi:10.1002/jgrd.50122, 2013.

719 Conway, H., Gades, A., and Raymond, C. F.: Albedo of dirty snow during conditions of melt, Water Resour. Res.,
720 32, 1713–1718, doi:10.1029/96WR00712, 1996.

721 Dentener, F., Kinne, S., Bond, T., Boucher, O., Cofala, J., Generoso, S., Ginoux, P., Gong, S., Hoelzemann, J. J., Ito,
722 A., Marelli, L., Penner, J. E., Putaud, J.-P., Textor, C., Schulz, M., van der Werf, G. R., and Wilson, J.:
723 Emissions of primary aerosol and precursor gases in the years 2000 and 1750 prescribed data-sets for
724 AeroCom, Atmos. Chem. Phys., 6, 4321–4344, doi:10.5194/acp-6-4321-2006, 2006.

725 Doherty, S. J., Dang, C., Hegg, D. A., Zhang, R., and Warren, S. G.: Black carbon and other light-absorbing
726 particles in snow of central North America, J. Geophys. Res. Atmos., 119, 12,807–12,831,
727 doi:10.1002/2014JD022350, 2014.

728 Duan, A., Wu G., Zhang Q., and Liu Y.: New proofs of the recent climate warming over the Tibetan Plateau as a
729 result of the increasing greenhouse gases emissions, Chin. Sci. Bull., 51, 1396–1400, doi:10.1007/s11434-
730 006-1396-6, 2006.

731 Duan, A. M. and Wu G. X.: Weakening trend in the atmospheric heat source over the Tibetan Plateau during recent
732 decades. Part I: Observations, J. Clim., 21, 3149–3164, doi:10.1175/2007JCLI1912.1, 2008.

733 Flanner, M. G., Zender, C. S., Randerson, J. T., and Rasch, P. J.: Present day climate forcing and response from
734 black carbon in snow, J. Geophys. Res., 112, D11202, doi:10.1029/2006JD008003, 2007.

735 Flanner, M. G., Zender, C. S., Hess, P. G., Mahowald, N. M., Painter, T. H., Ramanathan, V., and Rasch, P. J.:
736 Springtime warming and reduced snow cover from carbonaceous particles, Atmos. Chem. Phys., 9, 2481–
737 2497, doi:10.5194/acp-9-2481-2009, 2009.

738 Gettelman, A., Liu, X., Ghan, S. J., Morrison, H., Park, S., Conley, A. J., Klein, S. A., Boyle, J., Mitchell, D. L., and
739 Li, J. L. F.: Global simulations of ice nucleation and ice supersaturation with an improved cloud scheme in
740 the Community Atmosphere Model, J. Geophys. Res., 115, D18216, doi:10.1029/2009jd013797, 2010.

741 Ginot, P., Dumont, M., Lim, S., Patris, N., Taupin, J.-D., Wagnon, P., Gilbert, A., Arnaud, Y., Marinoni, A.,
742 Bonasoni, P., and Laj, P.: A 10 year record of black carbon and dust from a Mera Peak ice core (Nepal):
743 variability and potential impact on melting of Himalayan glaciers, The Cryosphere, 8, 1479-1496,
744 doi:10.5194/tc-8-1479-2014, 2014.

745 Hadley, O. L. and Kirchstetter, T.W.: Black-carbon reduction of snow albedo, Nat. Clim. Change, 2, 437–440, 2012.

746 Hall, D. K., Riggs G. A., and Salomonson V. V.: updated monthly. MODIS/TERRA Snow Cover Monthly L3
747 Global 0.05Deg CMG V005, [2001], Boulder, CO, National Snow and Ice Data Center. Digital Media,
748 distributed in netCDF format by the Integrated Climate Data Center (ICDC, http://icdc.zmaw.de University
749 of Hamburg, Hamburg, Germany), 2006.

750 Hall, A. and Qu, X.: Using the current seasonal cycle to constrain snow albedo feedback in future climate change,
751 Geophys. Res. Lett., 33, L03502, doi:10.1029/2005GL025127, 2006.

752 Hansen, J. and Nazarenko, L.: Soot climate forcing via snow and ice albedos, P. Natl. Acad. Sci. USA, 101, 423–
753 428, doi:10.1073/pnas.2237157100, 2004.

754 Hansen, J., Sato, M., Ruedy, R., Nazarenko, L., Lacis, A., Schmidt, G. A., Russell, G., Aleinov, I., Bauer, M., Bauer,
755 S., Bell, N., Cairns, B., Canuto, V., Chandler, M., Cheng, Y., Del Genio, A., Faluvegi, G., Fleming, E.,
756 Friend, A., Hall, T., Jackman, C., Kelley, M., Kiang, N., Koch, D., Lean, J., Lerner, J., Lo, K., Menon, S.,
757 Miller, R., Minnis, P., Novakov, T., Oinas, V., Perlwitz, Ja., Perlwitz, Ju., Rind, D., Romanou, A., Shindell,
758 D., Stone, P., Sun, S., Tausnev, N., Thresher, D., Wielicki, B., Wong, T., Yao, M., and Zhang, S.: Efficacy
759 of climate forcings, J. Geophys. Res., 110, D18104, doi:10.1029/2005JD005776, 2005.

760 Huang, J., Minnis, P., Yi, Y., Tang, Q., Wang, X., Hu, Y., Liu, Z., Ayers, K., Trepte, C., and Winker, D.: Summer
761 dust aerosols detected from CALIPSO over the Tibetan Plateau, Geophys. Res. Lett., 34, L18805,
762 doi:10.1029/2007GL029938, 2007.

763 Huang, J., Fu, Q., Zhang, W., Wang, X., Zhang, R., Ye, H., and Warren, S. G.: Dust and black carbon in seasonal
764 snow across Northern China, Bull. Am. Meteorol. Soc., 92, 175–181, doi:10.1175/2010BAMS3064.1, 2011.

765 Hurrell, J. W., Holland, M. M., Ghan, S., Lamarque, J.-F., Lawrence, D., Lipscomb, W. H., Mahowald, N., Marsh,
766 D., Rasch, P., Bader, D., Collins, W. D., Gent, P. R., Hack, J. J., Kiehl, J., Kushner, P., Large, W. G.,
767 Marshall, S., Vavrus, S., and Vertenstein, M.: The Community Earth System Model: A Framework for
768 Collaborative Research, Bull. Am. Meteorol. Soc., 94, 1339-1360, doi:10.1175/BAMS-D-12-00121, 2013.

769 Immerzeel, W., VanBeek L. P. H., and Bierkens, M. F. P.: Climate Change Will Affect the Asian Water Towers,
770 Science, 328, 1382–1385, doi:10.1126/science.1183188, 2010.

771 Jacobson, M. Z.: Climate response of fossil fuel and biofuel soot, accounting for soot's feedback to snow and sea ice
772 albedo and emissivity, J. Geophys. Res., 109, D21201, doi:10.1029/2004JD004945, 2004.

773 Jiao, C., Flanner, M. G., Balkanski, Y., Bauer, S. E., Bellouin, N., Berntsen, T. K., Bian, H., Carslaw, K. S.,
774 Chin, M., De Luca, N., Diehl, T., Ghan, S. J., Iversen, T., Kirkevåg, A., Koch, D., Liu, X., Mann, G. W.,
775 Penner, J. E., Pitari, G., Schulz, M., Seland, Ø., Skeie, R. B., Steenrod, S. D., Stier, P., Takemura, T.,
776 Tsigaridis, K., van Noije, T., Yun, Y., and Zhang, K.: An AeroCom assessment of black carbon in Arctic
777 snow and sea ice, Atmos. Chem. Phys., 14, 2399-2417, doi:10.5194/acp-14-2399-2014, 2014.

778 Kang, S., Wake C., Qin. D., Mayewski P. A., and Yao T.: Monsoon and dust signals recorded in Dasuopu glacier,
779 Tibetan Plateau, J. Glaciol., 46(153), 222–226, 2000.

780 Kang, S., Wei, X., You, Q., Flugel, W., Pepin, N., and Yao, T.: Review of climate and cryospheric change in the
781 Tibetan Plateau, Environ. Res. Lett., 5, 015101, doi:10.1088/1748-9326/5/1/015101, 2010.

782 Kaser, G., Grosshauser, M., and Marzeion, B.: Contribution of glaciers to water availability in different climate
783 regimes, P. Natl. Acad. Sci. USA, 107, 20223–20227, doi:10.1073/pnas.1008162107, 2010

784 Kaspari, S. D., Schwikowski, M., Gysel, M., Flanner, M. G., Kang, S., Hou, S., and Mayewski, P. A.: Resent
785 increase in black carbon concentrations from a Mt. Everest ice core spanning 1860–2000 AD, Geophys.
786 Res. Lett., 38, L04703, doi:10.1029/2010GL046096, 2011.

787 Kopacz, M., Mauzerall, D. L., Wang, J., Leibensperger, E. M., Henze, D. K., and Singh, K.: Origin and radiative
788 forcing of black carbon transported to the Himalayas and Tibetan Plateau, Atmos. Chem. Phys., 11, 2837-
789 2852, doi:10.5194/acp-11-2837-2011, 2011.

790 Lamarque, J.-F., Bond, T. C., Eyring, V., Granier, C., Heil, A., Klimont, Z., Lee, D., Liousse, C., Mieville, A.,
791 Owen, B., Schultz, M. G., Shindell, D., Smith, S. J., Stehfest, E., Van Aardenne, J., Cooper, O. R.,
792 Kainuma, M., Mahowald, N., McConnell, J. R., Naik, V., Riahi, K., and van Vuuren, D. P.: Historical

(1850–2000) gridded anthropogenic and biomass burning emissions of reactive gases and aerosols: methodology and application, Atmos. Chem. Phys., 10, 7017–7039, doi:10.5194/acp-10-7017-2010, 2010.

Lamarque, J. F., Emmons, L. K., Hess, P. G., Kinnison, D. E., Tilmes, S., Vitt, F., Heald, C. L., Holland, E. A., Lauritzen, P. H., Neu, J., Orlando, J. J., Rasch, P. J., and Tyndall, G. K.: CAM-chem: description and evaluation of interactive atmospheric chemistry in the Community Earth System Model, Geosci. Model Dev., 5, 369–411, doi:10.5194/gmd-5-369-2012, 2012.

Lau, K. M., Kim, M. K., and Kim, K. M.: Asian monsoon anomalies induced by aerosol direct forcing: the role of the Tibetan Plateau, Clim. Dyn., 26, 855–664, 2006.

Lau, K.-M., Kim, M. K., Kim, K.-M., and Lee, W. S.: Enhanced surface warming and accelerated snow melt in the Himalayas and Tibetan Plateau induced by absorbing aerosols, Environ. Res. Lett., 5, 025204 doi:10.1088/1748-9326/5/2/025204, 2010.

Lee, Y. H., Lamarque, J.-F., Flanner, M. G., Jiao, C., Shindell, D. T., Berntsen, T., Bisiaux, M. M., Cao, J., Collins, W. J., Curran, M., Edwards, R., Faluvegi, G., Ghan, S., Horowitz, L. W., McConnell, J. R., Ming, J., Myhre, G., Nagashima, T., Naik, V., Rumbold, S. T., Skeie, R. B., Sudo, K., Takemura, T., Thevenon, F., Xu, B., and Yoon, J.-H.: Evaluation of preindustrial to present-day black carbon and its albedo forcing from Atmospheric Chemistry and Climate Model Intercomparison Project (ACCMIP), Atmos. Chem. Phys., 13, 2607-2634, doi:10.5194/acp-13-2607-2013, 2013.

Li, X., Cheng, G., Jin, H., Kang, E., Che, T., Jin, R., Wu, L., Nan, Z., Wang, J., and Shen, Y.: Cryospheric change in China, Global Planet. Change, 62(3–4), 210–218, 2008.

Liu, X., Easter, R. C., Ghan, S. J., Zaveri, R., Rasch, P., Shi, X., Lamarque, J.-F., Gettelman, A., Morrison, H., Vitt, F., Conley, A., Park, S., Neale, R., Hannay, C., Ekman, A. M. L., Hess, P., Mahowald, N., Collins,W., Iacono, M. J., Bretherton, C. S., Flanner, M. G., and Mitchell, D.: Toward a minimal representation of aerosols in climate models: description and evaluation in the Community Atmosphere Model CAM5, Geosci. Model Dev., 5, 709–739, doi:10.5194/gmd-5-709-2012, 2012.

Liu, Z., Liu, D., Huang, J., Vaughan, M., Uno, I., Sugimoto, N., Kittaka, C., Trepte, C., Wang, Z., Hostetler, C., and Winker, D.: Airborne dust distributions over the Tibetan Plateau and surrounding areas derived from the first year of CALIPSO lidar observations, Atmos. Chem. Phys., 8, 5045-5060, doi:10.5194/acp-8-5045-2008, 2008.

Lu, Z., Streets, D. G., Zhang, Q., and Wang, S.: A novel back-trajectory analysis of the origin of black carbon transported to the Himalayas and Tibetan Plateau during 1996–2010, Geophys. Res. Lett., 39, L01809, doi:10.1029/2011GL049903, 2012.

Ma, P.-L., Rasch, P. J., Wang, H., Zhang, K., Easter, R. C., Tilmes, S., Fast, J. D., Liu, X., Yoon, J.-H., and Lamarque, J.-F.: The role of circulation features on black carbon transport into the Arctic in the Community Atmosphere Model Version 5 (CAM5), J. Geophys. Res. - Atmos., 118, 4657–4669, 2013.

Manabe, S., and Terpstra T. B.: The effects of mountains on the general circulation of the atmosphere as identified by numerical experiments, J. Atmos. Sci., 31, 3–42, 1974.

Marinoni, A., Cristofanelli, P., Laj, P., Duchi, R., Calzolari, F., Decesari, S., Sellegri, K., Vuillermoz, E., Verza, G. P., Villani, P., and Bonasoni, P.: Aerosol mass and black carbon concentrations, a two year record at NCO-P (5079 m, Southern Himalayas), Atmos. Chem. Phys., 10, 8551–8562, doi:10.5194/acp-10-8551-2010, 2010.

833 Marinoni, A., Cristofanelli, P., Laj, P., Duchi, R., Putero, D., Calzolari, F., Landi, T. C., Vuillermoz, E., Maione, M.,
834 and Bonasoni, P.: High black carbon and ozone concentrations during pollution transport in the Himalayas:
835 Five years of continuous observations at NCO-P global GAW station, J. Environ. Sci., 25, 1618–1625,
836 doi:10.1016/S1001-0742(12)60242-3, 2013.

837 Ménégoz, M., Krinner, G., Balkanski, Y., Boucher, O., Cozic, A., Lim, S., Ginot, P., Laj, P., Gallée, H., Wagnon, P.,
838 Marinoni, A., and Jacobi, H. W.: Snow cover sensitivity to black carbon deposition in the Himalayas: from
839 atmospheric and ice core measurements to regional climate simulations, Atmos. Chem. Phys., 14, 4237-
840 4249, doi:10.5194/acp-14-4237-2014, 2014.

841 Menon, S., Koch, D., Beig, G., Sahu, S., Fasullo, J., and Orlikowski, D.: Black carbon aerosols and the third polar
842 ice cap, Atmos. Chem. Phys., 10, 4559–4571, doi:10.5194/acp-10-4559-2010, 2010.

843 Ming, J., Cachier, H., Xiao, C., Qin, D., Kang, S., Hou, S., and Xu, J.: Black carbon record based on a shallow
844 Himalayan ice core and its climatic implications, Atmos. Chem. Phys., 8, 1343–1352, doi:10.5194/acp-8-
845 1343-2008, 2008.

846 Ming, J., Xiao, C. D., Cachier, H., Qin, D. H., Qin, X., Li, Z. Q., and Pu, J. C.: Black carbon (BC) in the snow of
847 glaciers in west China and its potential effects on albedos, Atmos. Res., 92, 114–123,
848 doi:10.1016/j.atmosres.2008.09.007, 2009.

849 Ming, J., Xiao C., Sun J., Kang S., and Bonasoni P.: Carbonaceous particles in the atmosphere and precipitation of
850 the Nam Co region, central Tibet, J. Environ. Sci., 22(11), 1748–1756, doi:10.1016/S1001-0742(09)60315-
851 6, 2010.

852 Ming, J., Xiao, C., Du, Z., and Yang, X.: An overview of black carbon deposition in High Asia glaciers and its
853 impacts on radiation balance, Adv. Water Resour., 55, 80–87, 2013.

854 Moorthy, K. K., Beegum, S. N., Srivastava, N., Satheesh, S. K., Chin, M., Blond, N., Babu, S. S., and Singh, S.:
855 Performance evaluation of chemistry transport models over India, Atmos. Environ., 71, 210–225, 2013.

856 Neale, R. B., Chen, C.-C., Gettelman, A., Lauritzen, P. H., Park, S., Williamson, D. L., Conley, A. J., Garcia, R.,
857 Kinnison, D., Lamarque, J.-F., Marsh, D., Mills, M., Smith, A. K., Tilmes, S., Vitt, F., Cameron-Smith, P.,
858 Collins, W. D., Iacono, M. J., Easter, R. C., Ghan, S. J., Liu, X., Rasch, P. J., and Taylor, M. A.:
859 Description of the NCAR Community Atmosphere Model (CAM 5.0), NCAR/TN-486+STR, available at:
860 http://www.cesm.ucar.edu/models/cesm1.0/cam/docs/description/cam5_desc.pdf (last access: 26 December
861 2014), 2012.

862 Ohara, T., Akimoto, H., Kurokawa, J., Horii, N., Yamaji, K., Yan, X., and Hayasaka, T.: An Asian emission
863 inventory of anthropogenic emission sources for the period 1980–2020, Atmos. Chem. Phys., 7, 4419-4444,
864 doi:10.5194/acp-7-4419-2007, 2007.

865 Petzold, A., Ogren, J. A., Fiebig, M., Laj, P., Li, S.-M., Baltensperger, U., Holzer-Popp, T., Kinne, S.,
866 Pappalardo, G., Sugimoto, N., Wehrli, C., Wiedensohler, A., and Zhang, X.-Y.: Recommendations for
867 reporting "black carbon" measurements, Atmos. Chem. Phys., 13, 8365-8379, doi:10.5194/acp-13-8365-
868 2013, 2013.

869 Prasad, A. K. and Singh, R. P.: Changes in Himalayan Snow and Glacier Cover Between 1972 and 2000, Eos Trans.
870 AGU, 88, 33, doi:10.1029/2007EO330002, 2007.

871 Pu, Z., Xu L., and Salomonson V. V.: MODIS/Terra observed seasonal variations of snow cover over the Tibetan
872 Plateau, Geophys. Res. Lett., 34, L06706, doi:10.1029/2007GL029262, 2007.

873 Qian, Y., Flanner, M. G., Leung, L. R., and Wang, W.: Sensitivity studies on the impacts of Tibetan Plateau
874 snowpack pollution on the Asian hydrological cycle and monsoon climate, Atmos. Chem. Phys., 11, 1929-
875 1948, doi:10.5194/acp-11-1929-2011, 2011.

876 Qian, Y., Wang H., Zhang R., Flanner M. G., and Rasch P. J.: A sensitivity study on modeling black carbon in snow
877 and its radiative forcing over the Arctic and Northern China, Environ. Res. Lett., 9, 064001,
878 doi:10.1088/1748-9326/9/6/064001, 2014.

879 Qian, Y., Yasunari, T. J., Doherty, S. J., et al., Light-absorbing particles in snow and ice: measurement and
880 modeling of climatic and hydrological impact. *Adv. Atmos. Sci.*, 32(1), 64-91 doi: 10.1007/s00376-014-
881 0010-0, 2015.

882 Qin, D., Liu, S., and Li, P.: Snow cover distribution, variability, and response to climate change in western China, J.
883 Clim., 19(9), 1820–1833, 2006.

884 Qiu, J.: China: the third pole. Nature News, 454(7203), 393-396, 2008.

885 Ram, K., Sarin, M. M., and Hegde, P.: Long-term record of aerosol optical properties and chemical composition
886 from a high-altitude site (Manora Peak) in Central Himalaya, Atmos. Chem. Phys., 10, 11791–11803,
887 doi:10.5194/acp-10-11791-2010, 2010.

888 Ramanathan, V., Ramana, M. V., Roberts, G., Kim, D., Corrigan, C., Chung, C., Winker, D.: Warming trends in
889 Asia amplified by brown clouds solar absorption, Nature, 448, 575–578, 2007.

890 Rasch, P. J., Mahowald, N. M., and Eaton, B. E.: Representations of transport, convection, and the hydrological
891 cycle in chemical transport models: Implications for the modeling of short-lived and soluble species, J.
892 Geophys. Res., 102, 28 127–28 138, 1997.

893 Ren, J., Jing, Z., Pu, J., and Qin, X.: Glaciers variations and climate change in the central Himalaya over the past
894 few decades, Ann. Glaciol., 43, 218–222, 2006.

895 Rienecker, M. M., Suarez, M. J., Gelaro, R., Todling, R., Bacmeister, J., Liu, E., Bosilovich, M. G., Schubert, S. D.,
896 Takacs, L., Kim, G.-K., Bloom, S., Chen, J., Collins, D., Conaty, A., da Silva, A., Gu,W., Joiner, J., Koster,
897 R. D., Lucchesi, R., and Molod, A.: MERRA – NASA's Modern-Era Retrospective Analysis for Research
898 and Applications, J. Clim., 24, 3624–3648, 2011.

899 Singh, P. and Bengtsson, L.: Hydrological sensitivity of a large Himalayan basin to climate change, Hydrol. Process.,
900 18, 2363–2385, 2004.

901 Taylor, K. E., Stouffer, R. J., and Meehl, G. A.: An Overview of CMIP5 and the Experiment Design, Bull. Am.
902 Meteorol. Soc., 93, 485–498, doi:10.1175/BAMS-D-11-00094.1, 2012.

903 Wang, B., Bao, Q., Hoskins, B., Wu, G., and Liu, Y.: Tibetan Plateau warming and precipitation changes in East
904 Asia, Geophys. Res. Lett., 35, L14702, doi:10.1029/2008GL034330, 2008.

905 Wang, H., Easter, R. C., Rasch, P. J., Wang, M., Liu, X., Ghan, S. J., Qian, Y., Yoon, J.-H., Ma, P.-L., and Vinoj, V.:
906 Sensitivity of remote aerosol distributions to representation of cloud–aerosol interactions in a global
907 climate model, Geosci. Model Dev., 6, 765–782, doi:10.5194/gmd-6-765-2013, 2013.

908 Wang, H., Rasch, P. J., Easter, R. C., Singh, B., Zhang, R., Ma, P. L., Qian, Y., and Beagley, N.: Using an explicit
909 emission tagging method in global modeling of source-receptor relationships for black carbon in the Arctic:

910 Variations, Sources and Transport pathways, J. Geophys. Res.-Atmos., 119, 12888–12909, doi:
911 10.1002/2014JD022297, 2014.

912 Wang, M., Xu, B., Cao, J., Tie, X., Wang, H., Zhang, R., Qian, Y., Rasch, P. J., Zhao, S., Wu, G., Zhao, H.,
913 Joswiak, D. R., Li, J., and Xie, Y.: Carbonaceous aerosols recorded in a southeastern Tibetan glacier:
914 analysis of temporal variations and model estimates of sources and radiative forcing, Atmos. Chem. Phys.,
915 15, 1191-1204, doi:10.5194/acp-15-1191-2015, 2015.

916 Wang, X., S. J. Doherty, and J. Huang: Black carbon and other light-absorbing impurities in snow across Northern
917 China, J. Geophys. Res. Atmos., 118, 1471–1492, doi:10.1029/2012JD018291, 2013.

918 Warren, S. G. and Wiscombe,W. J.: A model for the spectral albedo of snow. II: Snow containing atmospheric
919 aerosols, J. Atmos. Sci., 37, 2734–2745, 1980.

920 Warren, S. G. and Wiscombe, W. J.: Dirty snow after nuclear war, Nature, 313, 469–470, 1985.

921 Wu, G., Liu, Y., He, B., Bao, Q., Duan, A., and Jin, F.-F.: Thermal controls on the Asian summer monsoon, Sci.
922 Rep., 2, 404, doi:10.1038/srep00404, 2012.

923 Xia, X. G., Zong, X. M., Cong, Z. Y., Chen, H. B., Kang, S. C., and Wang, P. C.: Baseline continental aerosol over
924 the central Tibetan plateau and a case study of aerosol transport from South Asia, Atmos. Environ., 45,
925 7370–7378, 2011.

926 Xu, B., Cao, J., Hansen, J., Yao, T., Joswiak, D. R., Wang, N.,Wu, G., Wang, M., Zhao, H., Yang, W., Liu, X., and
927 He, J.: Black soot and the survival of Tibetan glaciers, Proc. Natl. Acad. Sci. USA, 106, 22114–22118,
928 2009.

929 Xu, X., Lu C., Shi X., and Gao S.: World water tower: An atmospheric perspective, Geophys. Res. Lett., 35, L20815,
930 doi:10.1029/2008GL035867, 2008.

931 Yanai, M., Li, C., and Song, Z.: Seasonal heating of the Tibetan Plateau and its effects on the evolution of the Asian
932 summer monsoon, Journal of the Meteorological Society of Japan, 70, 319–351, 1992.

933 Yao, T., Pu, J., Lu, A., Wang, Y., and Yu, W.: Recent glacial retreat and its impact on hydrological processes on the
934 Tibetan Plateau, China, and surrounding regions, Arct. Antarct. Alp. Res., 39(4), 642–650, 2007.

935 Yao, T., Thompson, L., Yang, W., Yu, W., Gao, Y., Guo, X., Yang, X., Duan, K., Zhao, H., Xu, B., Pu, J., Lu, A.,
936 Xiang, Y., Kattel, D. B., and Joswiak, D.: Different glacier status with atmospheric circulations in Tibetan
937 Plateau and surroundings, Nat. Clim. Change, 2, 663–667, doi:10.1038/nclimate1580, 2012.

938 Yasunari, T. J., Bonasoni, P., Laj, P., Fujita, K., Vuillermoz, E., Marinoni, A., Cristofanelli, P., Duchi, R., Tartari,
939 G., and Lau, K.-M.: Estimated impact of black carbon deposition during premonsoon season from Nepal
940 Climate Observatory – Pyramid data and snow albedo changes over Himalayan glaciers, Atmos. Chem.
941 Phys., 10, 6603–6615, doi:10.5194/acp-10-6603-2010, 2010.

942 Ye, D. and Gao, Y.: Meteorology of the Qinghai-Xizang Plateau (Chinese Science Press, Beijing, 1979).

943 Ye, D. and Wu G.: The role of the heat source of the Tibetan Plateau in the general circulation, Meteorol. Atmos.
944 Phys., 67, 181–198, doi:10.1007/BF01277509, 1998.

945 Ye, H., Zhang, R., Shi, J., Huang, J., Warren, S. G., and Fu, Q.: Black carbon in seasonal snow across northern
946 Xinjiang in northwestern China, Environ. Res. Lett. 7, 044002, doi:10.1088/1748-9326/7/4/044002, 2012.

947 Yeh, T., Lo, S., and Chu P.: The wind structure and heat balance in the lower troposphere over Tibetan Plateau and
948 its surrounding. Acta Meteor. Sinica 28, 108–121, 1957.

949 Zhang, R., Hegg, D. A., Huang, J., and Fu, Q.: Source attribution of insoluble light-absorbing particles in seasonal
950 snow across northern China, Atmos. Chem. Phys., 13, 6091-6099, doi:10.5194/acp-13-6091-2013, 2013.

951 Zhang, X. Y., Arimoto, R., Cao, J. J., An, Z. S., and Wang, D.: Atmospheric dust aerosol over the Tibetan Plateau, J.
952 Geophys. Res., 106(D16), 18 471–18 476, 2001.

953 Zhao, S., Ming, J., Xiao, C., Sun, W., and Qin, X.: A preliminary study on measurements of black carbon in the
954 atmosphere of northwest Qilian Shan. J. Environ. Sci., 24(1), 152-159, doi:10.1016/S1001-0742(11)60739-
955 0, 2012.

956 Zhao, Z., Cao, J., Shen, Z., Xu, B., Chen, L- W. A., Ho, K., Han, Y., Zhu, C., and Liu, S.: Aerosol particles at a
957 high-altitude site on the Southeast Tibetan Plateau, China: implications for pollution transport from South
958 Asia, J. Geophys. Res.-Atmos., 118, 11360–11375, doi:10.1002/jgrd.50599, 2013.

959

**Table 1.** List of sites for the observations of atmospheric BC surface concentrations used in this study to evaluate our model simulation.

| Site | Latitude (°N) | Longitude (°E) | Elevation (m) | | Sampling time | Observation method | Contributor |
|---|---|---|---|---|---|---|---|
| | | | observation | model | | | |
| **Muztagh Ata** | 38.3 | 75.0 | 4500 | 3497 | 2003−2006 | Thermal Optical Reflectance (TOR) | Cao et al., 2009 |
| **Hanle** | 32.8 | 79.0 | 4250 | 4862 | 2009−2010 | Aethalometer | Babu et al., 2011 |
| **Manora Peak** | 29.4 | 79.5 | 1950 | 1409 | 2005−2008 | Thermal Optical Transmittance (TOT) | Ram et al., 2010 |
| **NCO-P** | 28.0 | 86.8 | 5079 | 4604 | 2006−2008 | Multi-angle absorption photometer (MAAP) | Marinoni et al., 2010 |
| **Lulang** | 29.5 | 94.4 | 3300 | 3370 | 2008−2009 | TOR | Zhao et al., 2013 |
| **NCOS** | 30.8 | 91.0 | 4730 | 4956 | 2006−2007 | TOR | Ming et al., 2010 |
| **QSSGEE** | 39.5 | 96.5 | 4214 | 2748 | 2009−2011 | Aethalometer | Zhao et al., 2012 |

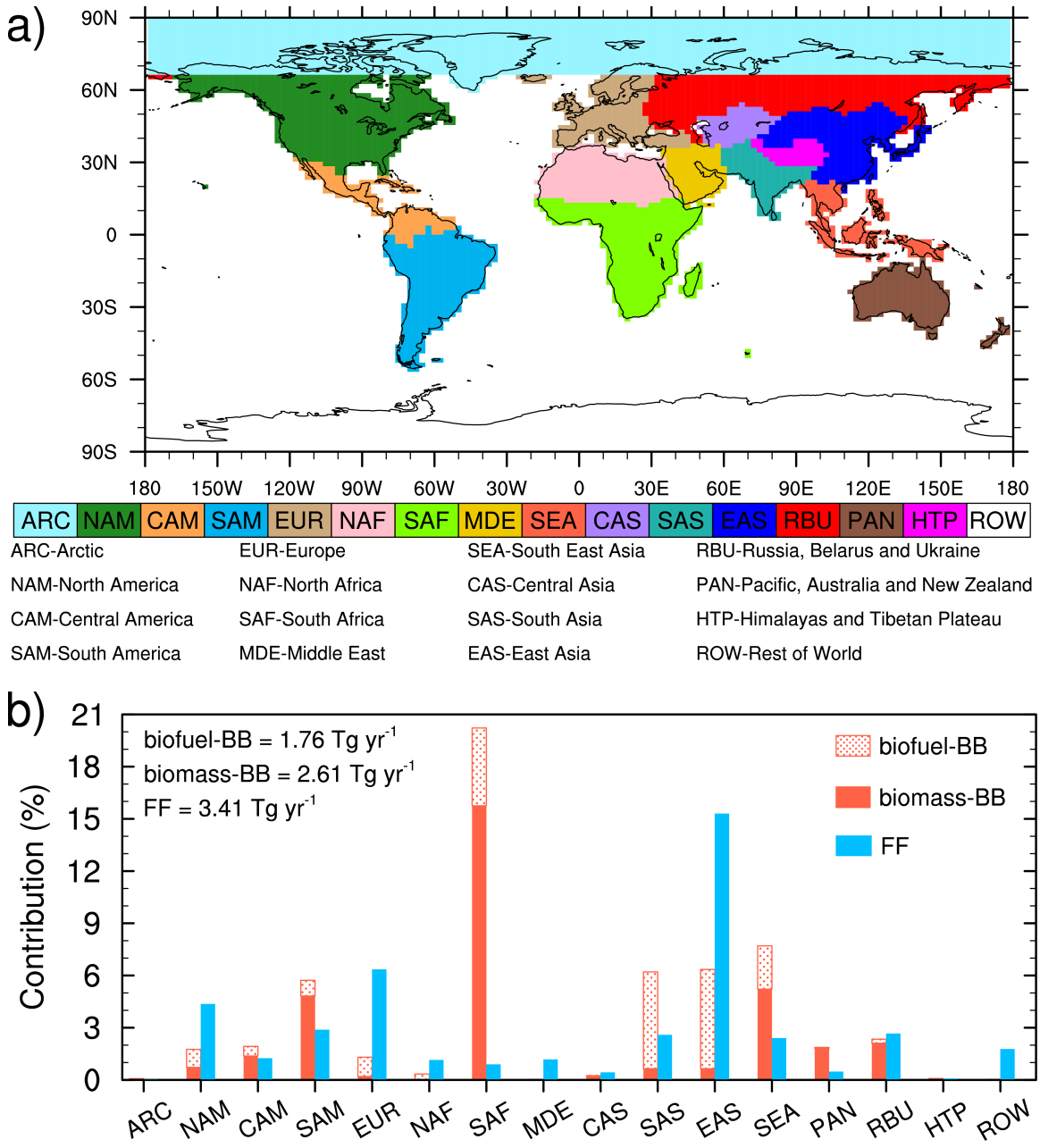


**Fig. 1.** (a) Tagged source regions and (b) the respective percentage contributions to global annual mean BC emissions from the individual source regions and sectors (including biofuel, biomass burning and fossil fuel). The global annual mean BC emission rate is 7.78 Tg $yr^{-1}$, which is divided up into the three sectors as indicated by the numbers at the upper-left corner.

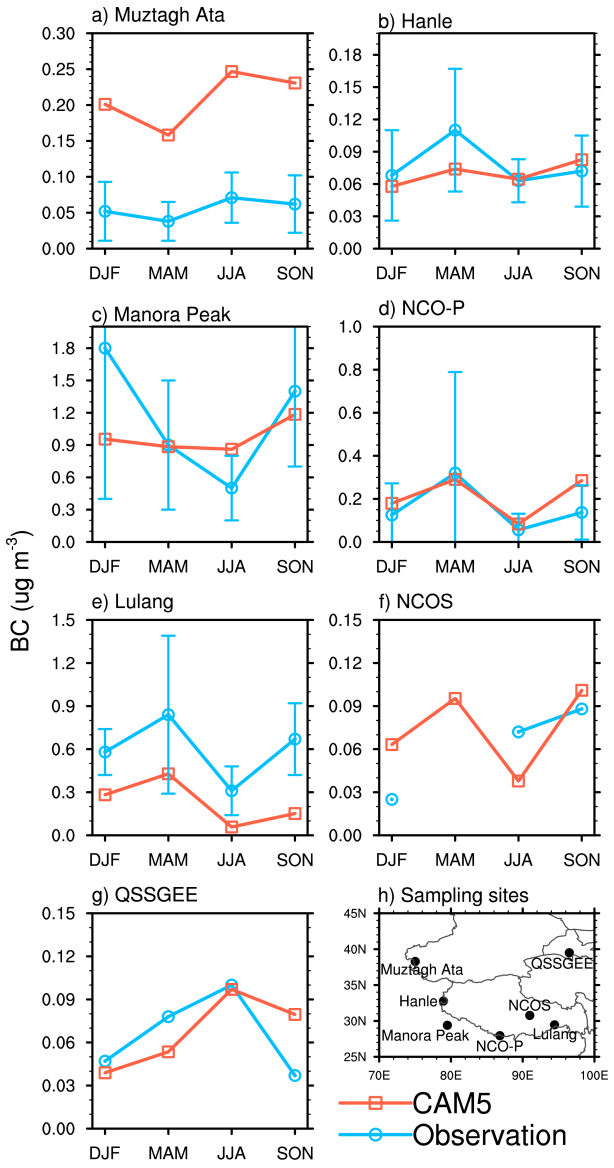


**Fig. 2.** Seasonal mean surface BC concentration (μg $m^{-3}$) from observations (blue lines with error bars denoting SD) and CAM5 simulation (red lines) at the seven sampling sites listed in Table 1 and marked in map of panel h.

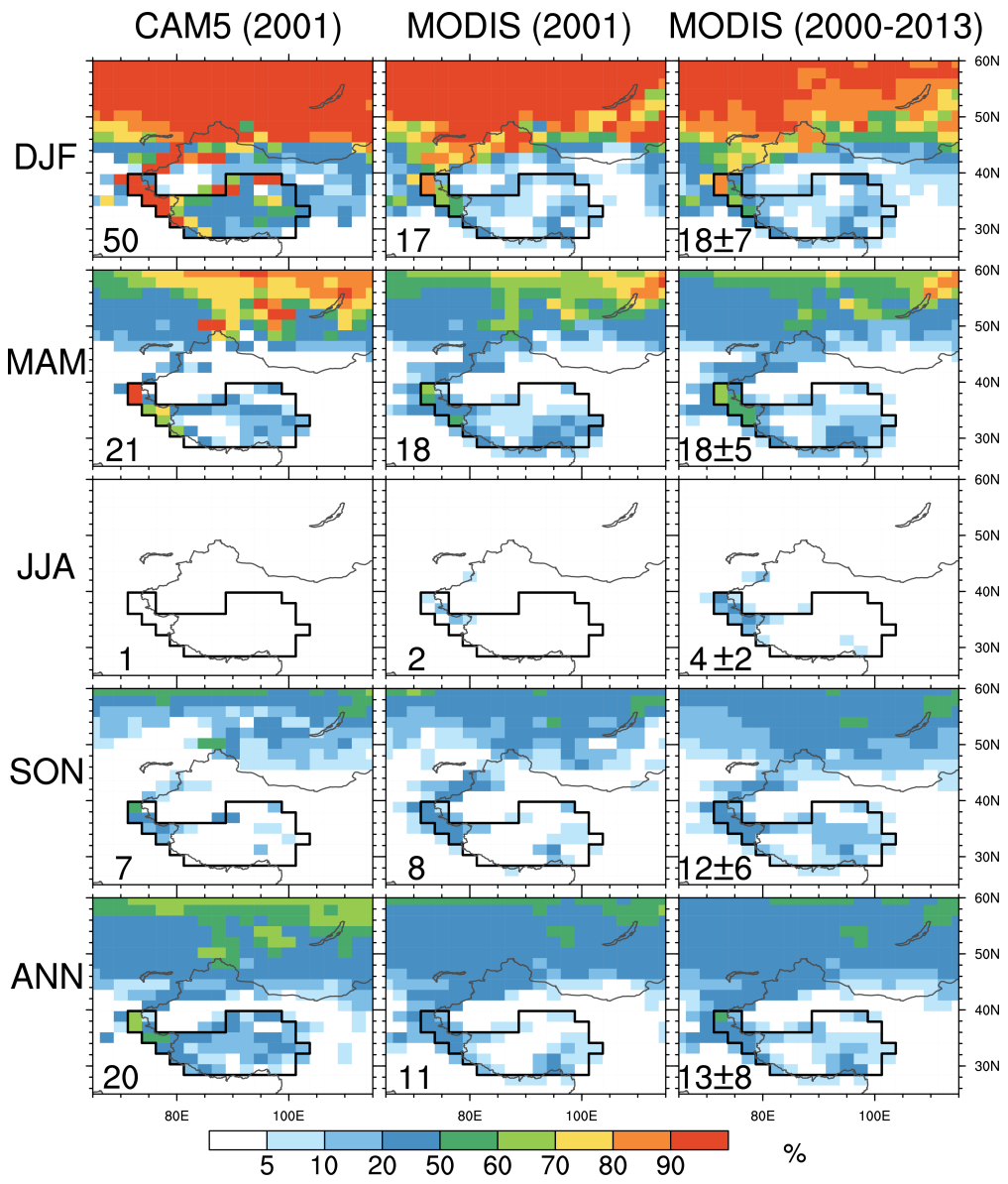


**Fig. 3.** Seasonal and annual mean snow cover fraction from CAM5 simulation for year 2001 (left), and MODIS retrieval for 2001 (middle) and 2000-2013 (right). The summer (JJA) in 2001 for both CAM5 and MODIS only includes July and August due to missing MODIS data in June. The number in the lower-left corner of each panel is the corresponding spatial mean SCF for the HTP region (which is marked with black outline), and for MODIS the standard deviation calculated from the MODIS multi-year means is also included.

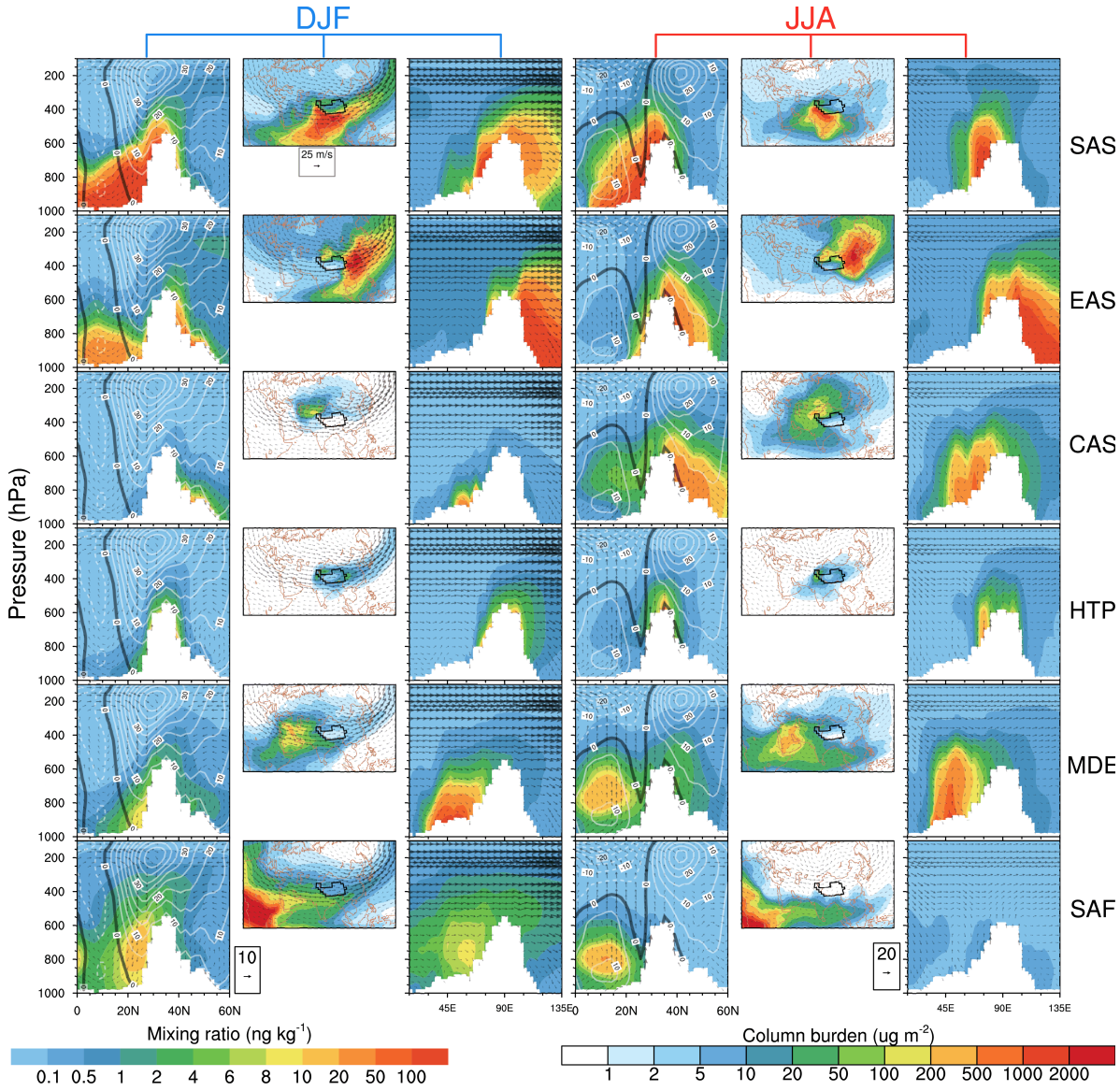


**Fig. 4.** The first column shows the latitude-height distributions of DJF BC mass mixing ratios (in ng $kg^{-1}$, colors) averaged over 71.25−101.25°E, originating from BB and FF sectors in the tagged source regions (corresponding to different rows); the white shaded area denotes topography, and the superimposed white contours at intervals of 5 m $s^{-1}$ represent the westerly (solid) and easterly (dashed) DJF mean zonal winds along the cross-section with the thick solid black contour at 0 m $s^{-1}$; the wind vectors (consisting of vertical velocity in units of $-10^{-4}$ hPa $s^{-1}$ and meridional wind in m $s^{-1}$) are represented by arrows. Colors in the second column denote spatial distribution of the DJF mean BC column burden (in μg $m^{-2}$), originating from different source regions, and the arrows represent the DJF mean horizontal wind vectors at 500hPa; the HTP is marked with black outline. The third column is similar to the first column except that the quantities are on the longitude-height cross-section averaged over 28−40°N, and thus the horizontal component of the wind vectors is zonal wind (m $s^{-1}$) instead. The fourth to sixth columns are the same as the first to third columns, respectively, but for JJA means instead.

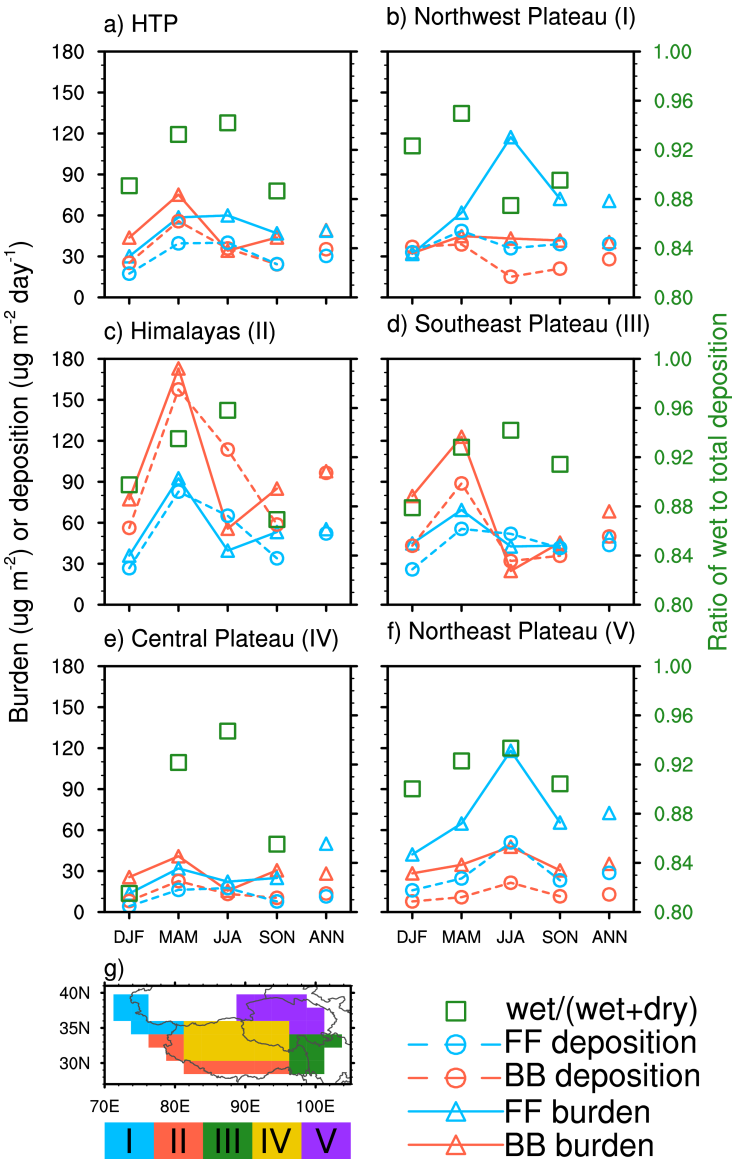


**Fig. 5.** Seasonal and annual mean BC column burden (solid lines and open triangles, in μg $m^{-2}$) and deposition rate (dashed lines and open circles, in μg $m^{-2}$ $day^{-1}$) over (a) the HTP, (b) Northwest Plateau, (c) Himalayas, (d) Southeast Plateau, (e) Central Plateau and (f) Northeast Plateau, emitted from BB (red color) and FF (blue color) source sectors. The green squares denote the ratio of wet to total BC deposition (using y-axis on the right) in four seasons over each receptor region. The geographical locations of five sub-regions of HTP are indicated in panel g.

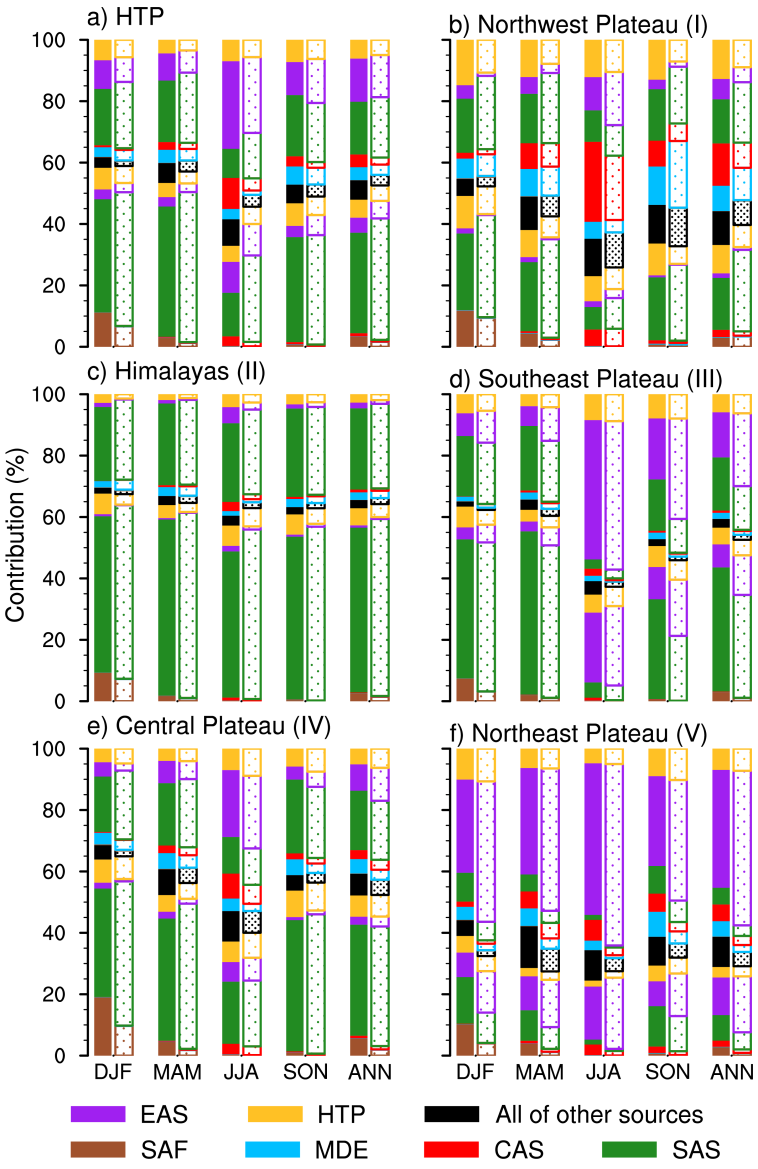


**Fig. 6.** Fractional contributions (measured by the lengths of color bars) to seasonal and annual mean BC column burden (solid pattern bars) and deposition (dotted pattern bars) over (a) the HTP, (b) Northwest Plateau, (c) Himalayas, (d) Southeast Plateau, (e) Central Plateau, and (f) Northeast Plateau, originating from six major tagged source regions (indicated by colors at the bottom) for BB (colors below the black bar) and FF (colors above the black color) emissions. The black bar in each column represents the contribution from all of the other tagged source regions and sectors.

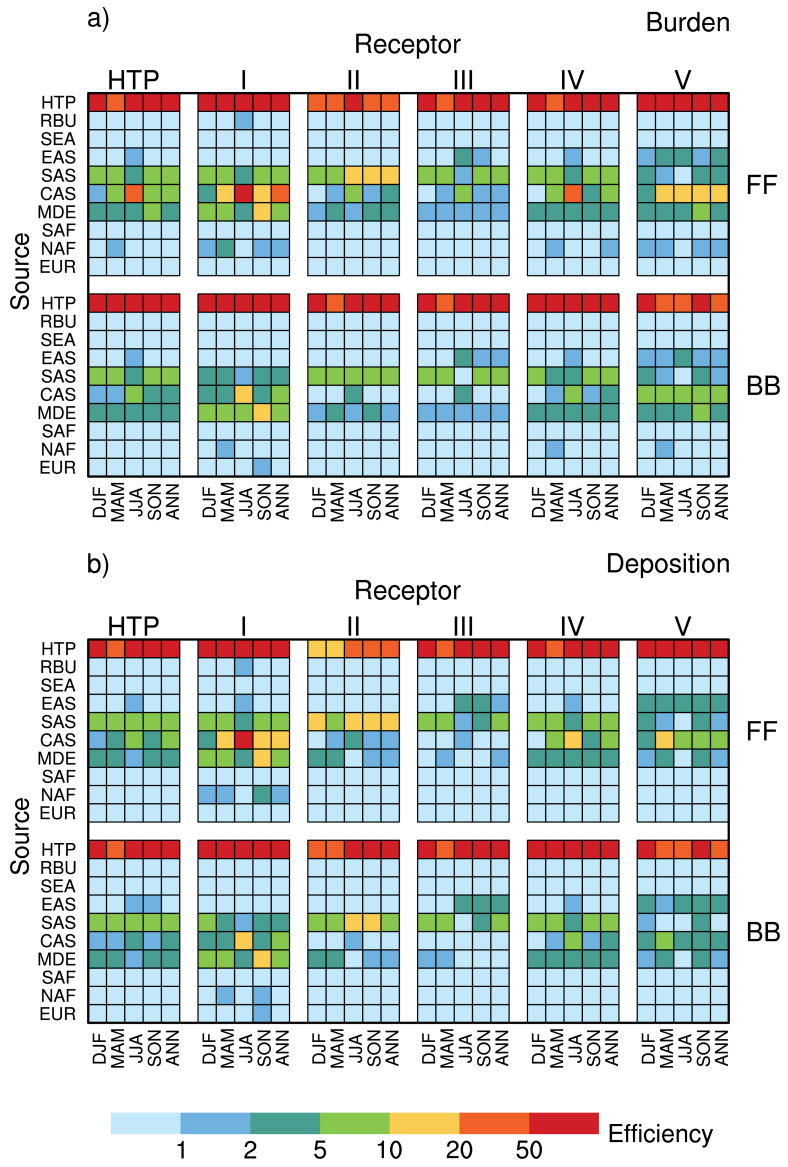


**Fig. 7.** Efficiency of FF (top) and BB (bottom) emissions from ten source regions (on the y-axis) in changing seasonal and annual mean (a) BC column burden and (b) deposition over the HTP and each of the five sub-regions: Northwest Plateau (I), Himalayas (II), Southeast Plateau (III), Central Plateau (IV) and Northeast Plateau (V).

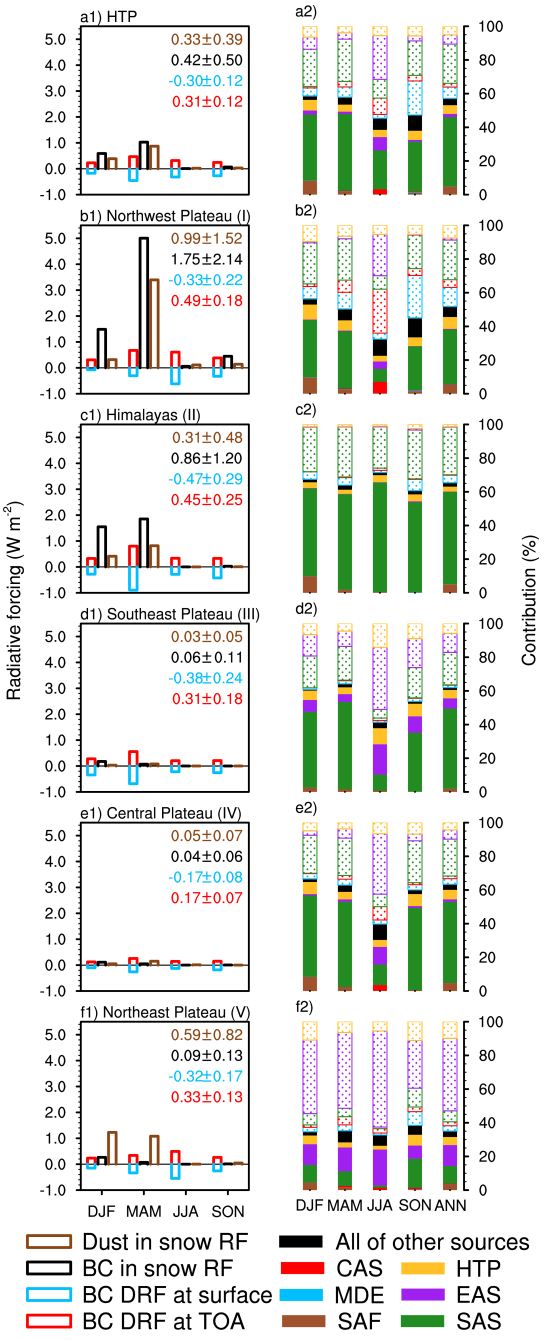


**Fig. 8.** Seasonal mean radiative forcing (left column) induced by the various BC effects (indicated by the color legend at the bottom) and dust-in-snow effect over (a1) the HTP, (b1) Northwest Plateau, (c1) Himalayas, (d1) Southeast Plateau, (e1) Central Plateau and (f1) Northeast Plateau. The corresponding annual mean forcings and one SD (for 12 monthly means) are shown in numbers on the top-right corner of each panel. The right column (a2-f2) panels represent source contribution to surface BC-in-snow radiative forcing over the corresponding receptors from tagged source regions (colors) and sectors (solid pattern bar and dotted pattern bar for BB and FF, respectively). The black bar in each column represents the contribution from all of the other tagged source regions and sectors.